applied sciences

MDPI

Article

Finite Elements for Higher Order Steel–Concrete Composite Beams

Fabrizio Gara [1,*], Sandro Carbonari [1], Graziano Leoni [2] and Luigino Dezi [1]

[1] DICEA—Department of Construction, Civil Engineering and Architecture, Università Politecnica delle Marche, 60121 Ancona, Italy; s.carbonari@univpm.it (S.C.); l.dezi@univpm.it (L.D.)
[2] SAAD—School of Architecture and Design, University of Camerino, 63100 Ascoli Piceno, Italy; graziano.leoni@unicam.it
* Correspondence: f.gara@univpm.it; Tel.: +39-071-220-4550

Featured Application: The paper presents finite elements for a higher order steel–concrete composite beam model that can be implemented within commercial software for structural analysis and used for the design of composite bridges.

Abstract: This paper presents finite elements for a higher order steel–concrete composite beam model developed for the analysis of bridge decks. The model accounts for the slab–girder partial interaction, the overall shear deformability, and the shear-lag phenomenon in steel and concrete components. The theoretical derivation of the solving balance conditions, in both weak and strong form, is firstly addressed. Then, three different finite elements are proposed, which are characterised by (i) linear interpolating functions, (ii) Hermitian polynomial interpolating functions, and (iii) interpolating functions, respectively, derived from the analytical solution expressed by means of exponential matrices. The performance of the finite elements is analysed in terms of the solution convergence rate for realistic steel–concrete composite beams with different restraints and loading conditions. Finally, the efficiency of the beam model is shown by comparing the results obtained with the proposed finite elements and those achieved with a refined 3D shell finite element model.

Keywords: beam finite element; consistent interpolation; higher order steel–concrete composite beam; interdependent interpolation; shear deformability; shear-lag

Citation: Gara, F.; Carbonari, S.; Leoni, G.; Dezi, L. Finite Elements for Higher Order Steel–Concrete Composite Beams. *Appl. Sci.* **2021**, *11*, 568. https://doi.org/10.3390/app11020568

Received: 18 December 2020
Accepted: 4 January 2021
Published: 8 January 2021

1. Introduction

Steel–concrete composite bridge decks are employed worldwide over medium span viaducts and bridges owing to their versatility and capability of properly exploiting peculiar material properties. Among several typologies, the most common are characterised by structural steel twin-girders or U-shaped girders connected by means of stud shear connectors to wide-cast in situ reinforced concrete slabs. Structural steel components are used to resist tensile stresses and vertical shear forces, whereas the concrete slab is used to resist compression stresses; as for torsion, this is resisted with different mechanisms depending on the overall cross-section layout (twin-girder or box-girder). Furthermore, the concrete slab guarantees a great in-plane stiffness.

The design of steel–concrete composite bridge decks requires to assess the structure behaviour with respect to both serviceability and ultimate limit states [1]; these include the control of the deflection under traffic loads and of stresses in both the steel plates and the concrete slab; furthermore, fatigue assessment of structural steel components and shear connectors has to be carried out. An accurate design of composite bridge decks generally requires refined finite element models, often based on shell elements, with high costs in terms of time to develop the model and run the analysis. On the contrary, analytical models (e.g., 1D beam models) have the merit of requiring a less important computational effort,

making it possible to investigate alternative design solutions, especially in the preliminary calculations aimed at sizing and optimizing the steel girders.

To provide sufficiently accurate results, theoretical models have to account for several peculiarities that characterize the behaviour of steel–concrete composite bridge decks. For straight beams, the most important issues are (i) the longitudinal deformability of steel connectors, which implies a partial interaction between the concrete slab and steel girder; (ii) the shear deformability of the composite cross section, which significantly affects the deflection for vertical loads, especially in the case of multi-supported continuous beams; and (iii) the in-plane shear deformability of the concrete slab and the flanges of the structural steel girder, which causes a non-uniform distribution of normal stresses within the elements (i.e., shear-lag effects). A wide range of scientific-technical literature covering all features relevant to design and modelling of composite systems is available nowadays. A state-of-the-art review is beyond the scope of this work and only a brief overview of some important papers selected among those published over the last two decades is presented in the following to introduce topics involved in this paper.

The composite beam model proposed in this paper is among those aimed at capturing the effects of the shear connection deformability. A pioneering work about this topic was done by Newmark [2], who described the partial interaction behaviour of a composite beam by considering two Euler–Bernoulli beams connected with a shear deformable layer. The Newmark model was used to investigate many features connected to particular material properties such as the time-dependent behavior of the concrete and the nonlinear behavior of materials or of the shear connection. Among many other authors, Nguyen et al. [3] proposed a 1D finite element for beams subjected to bending in which the concrete of the slab is assumed to be an age-dependent viscoelastic material; the solution is achieved in the time domain by means of a step-by-step integration and in the space domain by exploiting the exact closed form of the stiffness matrix. Ranzi and Bradford [4] adopted a closed form solution of the problem of composite beams subjected to transverse load in the framework of the direct stiffness method by adopting algebraic expressions for the time-dependent stress–strain concrete constitutive relationships. Gara et al. [5] investigated the effectiveness of various integration techniques in the space domain (finite elements, finite differences, direct stiffness, and exact solution), focusing on the discretization needed to get converge and to limit errors below established thresholds; even in this case, beams subjected to transverse loads are considered by adopting the age-adjusted effective modulus method to take into account the concrete creep. The Newmark model was demonstrated to also be very versatile in analyzing the effects of construction phases of bridges; Dezi et al. [6] proposed a model capable of accounting for creep and shrinkage of the early age concrete, as well as for the complex change of the static scheme due to the fractionated slab pouring by means of a step-by-step time integration procedure. Gara et al. [7] exploited the Newmark model in combination with specific time-dependent concrete effective modulus to investigate the effectiveness of various casting techniques in order to avoid early cracking of concrete slabs in composite bridges. Another field deeply investigated by means of the Newmark model is the nonlinear behavior of composite beams. Ranzi and Bradford [8] proposed a direct stiffness approach in an iterative procedure based on the secant stiffness method; the model was validated against several experimental cases, focusing on discretization issues. Among others, Virtuoso and Vieira [9] also investigated the combined effects of mechanical nonlinearity and time-dependent behavior of concrete. Dall'Asta and Zona [10] proposed a mixed finite element formulation for the nonlinear analysis of composite beams to improve the solution for problems usually characterized by bad convergence of usual finite element approaches.

Typical kinematic assumptions of the Newmark beam model were progressively relaxed, improving the analysis capabilities and the accuracy of new models. The first improvements regard the connection system, for which the multidirectional behaviour was introduced into 1D beam models; among others, Gara et al. [11] and Ranzi et al. [12] developed finite elements for two-layered composite beams capable of accounting for the

deformability of the slab–girder shear connection in the longitudinal and transverse-vertical directions. Partial interaction in both the longitudinal and transverse-lateral directions was instead introduced by Taig and Ranzi [13] in a very sophisticated model capable of capturing the behavior of elements such as bridge composite box girders, in which cross-section deformation occurs. Discrete connections were also considered by Nguyen et al. [14] by considering friction arising at the interface of the two components in the contact areas. Zero-thickness interface elements were developed by da Silva and Suasa [15] to account for partial composite actions in the simulation of steel–concrete composite elements, layered beams, or other structural systems in which components are connected with the possibility of interlayer slip.

One of the features that makes the Newmark model sometimes inaccurate is neglecting the shear deformability of elements [16]. The solution of partial interaction composite beams based on the Timoshenko beam theory [17] was discussed by Xu and Wang in [18], pointing out when the evaluation of the flexural-slip-shear deformation is affected by shear deformability of components. The static behavior of composite beams with refined shear deformation theories is presented by Vo and Thai [19], accounting for all coupling coming from the material anisotropy of layers composing the beam. Zona and Ranzi [20] proposed finite element models for the nonlinear analysis of steel concrete composite beams, in which Timoshenko beams are used for both the steel and concrete elements, and pointed out situations in which the interaction between bending and shear plays a substantial role. Nguyen et al. [14] developed a finite element for shear-deformable two-layer beams by exploiting exact stiffness matrices derived by analytical solutions of the problem. Ranzi and Zona [21] proposed a steel–concrete composite beam model with partial interaction in which a Timoshenko element was used for the steel component; by means of a wide parametric analysis, they determined conditions requiring the modelling of the shear deformation of the steel components. An analytical solution of two-layer beam was derived by Schnabl et al. [22] considering the interlayer slip and the shear deformation of elements, demonstrating their importance for high shear connection stiffness, for beams with small length/height ratios, and for beams with high normal/shear moduli ratios.

As known, for composite systems characterized by elements with a high width/thickness ratio, the assumption of preservation of plane cross section, on which the Bernoulli and Timoshenko theories are based, is no longer valid, and warping of cross section was introduced by many researchers to capture nonuniform stress distributions within the elements. Dezi et al. [23] proposed a theoretical model for steel concrete composite bridge decks by including shear lag in the reinforced concrete slab and partial interaction between steel and concrete components; the same authors [24] demonstrated how the shear lag phenomenon is important over the whole length of the beam, mainly when vertical loads are applied, whereas shrinkage and other kinds of actions like support settlements and prestressing produce effects only in limited regions [25]. Macorini et al. [26] proposed a finite element analysis to evaluate long-term concrete slab effective width by also considering the concrete cracking in hogging regions (i.e., with negative bending moments). Gara et al. demonstrated the versatility of a specific finite element derived by the theoretical model in analyzing real structural systems like cabled stayed bridges [27] or arch bridges [28].

The most recent and advanced models, in terms of enhanced kinematics, are those developed in the framework of the generalized beam theory and those denoted as higher order models. Taig and Ranzi [13] presented a two-layer composite beam model capable of capturing cross-sectional deformations and partial interaction in both the longitudinal and transverse directions by introducing a set of deformation modes derived by modal analysis of planar frames representing the cross sections. Similarly, Gonçalves and Camotim [29] presented a model able to capture the effects of cross-sectional deformation for a wide range of analyses including vibration and lateral-torsional-distortional buckling of composite cross sections typical for bridge applications. Gara et al. [30] presented a higher order model suitable for the analysis of composite bridge decks accounting for the overall shear deformability, warping of the slab cross section and of the steel beam, and partial shear

interaction. Chakrabarti et al. [31] proposed a finite element beam model that includes shear warping and considers longitudinal and vertical partial interaction between the components.

As also mentioned in the above discussion, solving methods can be roughly divided into two large classes: (i) methods providing the "exact" solution, such as closed-form expressions or analytical formulations such exponential matrix method; and (ii) methods providing approximated solutions, such as the finite difference method and the finite element method. Despite their name, "exact" solutions are affected by approximations due to precision of calculators and often by numerical issues deriving from the adopted algorithms; furthermore, analytical solutions, especially the closed-form ones, are only available for specific cases (e.g., specific geometric, loading, and restraint conditions). On the other hand, numerical solutions, although approximated, offer a wider versatility, being able to account for generic geometry as well as generic restraint systems and loading conditions. Before adopting a model with its relevant solving approach, it is imperative to know not only its theoretical applicability, but also the expected degree of approximation of the solution. The latter depends not only on the accuracy of the analytical model, because of the assumed admissible displacement field, but also on the numerical approach adopted for the solution (e.g., locking problems for finite elements).

A further issue is the efficiency of the numerical approach to achieve a desired degree of precision, which reflects on the computation time depending on the refinement of the geometric discretization and the computation capacity.

In this paper, three new finite elements for the numerical solution of a theoretical higher order model developed by the authors [30] for the analysis of steel–concrete composite beams (Figure 1) are presented. The model, which accounts for the overall shear deformability and the shear-lag phenomenon on both steel and concrete members of composite beams, is firstly recalled providing a formulation that simplifies the subsequent numerical implementation. Both the kinematics (i.e., the assumed displacement field) and the active stresses field (according to linear elastic laws for the materials) are reported; the balance conditions in both weak and strong forms are provided.

(**a**) (**b**)

Figure 1. Examples of steel–concrete bridge decks: (**a**) continuous twin-girder multi-span viaduct-Serra Cazzola viaduct, AG, Italy; (**b**) continuous box-girder multi-span bridge on the Cesano River, at Mondolfo, PU, Italy.

Then, three finite elements characterised by different interpolating functions are developed, namely, a general finite element (*GFE*) (a 16 degrees of freedom (dof) element with linear shape functions); a consistent interpolation finite element (*CIFE*) (a 25 dof element with polynomial functions whose degree is chosen to avoid locking problems); and an interdependent interpolation finite element (*IIFE*), adopting shape functions derived from the closed-form solution.

The performance of the proposed finite elements is analysed in terms of the rate of convergence, considering realistic steel–concrete composite beams with different restraints and loading conditions and assuming as a benchmark the solution obtained with the *IIFE* and a refined discretization. Finally, the overall efficiency of the proposed beam model in capturing the behaviour of a composite bridge deck is shown by comparing the results of the model (implementing all the finite elements) with those achieved with a refined 3D finite element (FE) model developed with SAP2000® [32].

The theoretical higher order model for the analysis of composite beams is briefly recalled in Section 2 and different finite elements to solve the problem numerically are developed in Section 3, discussing their effectiveness as a function of the beam discretization. In Section 4, the overall efficiency of the beam model in capturing the behaviour of a composite bridge deck is shown through comparisons with the results from a refined three-dimensional FE model developed with a commercial software.

2. Recall of the Analytical Model

The analytical model by Gara et al. [30] is herein recalled, providing an alternative formulation to make the subsequent numerical implementation easier.

A generic prismatic steel–concrete composite beam of length L with a symmetric cross section is considered and an orthonormal global reference frame $\{0, X, Y, Z\}$, having the Z axis along the beam longitudinal direction, is assumed (Figure 2a); u, v, and w denote displacements along coordinate directions X, Y, and Z, respectively. The cross section is assumed to be symmetric with respect to the YZ plane; it is constituted by a concrete slab, with width B and thickness h_c, including longitudinal reinforcements and pre-stressing-wires, and by a steel girder. The connection between the reinforced concrete slab and steel girder is assumed to be uniformly distributed along lines at the coordinate $(\overline{x}_n, \overline{y})$, as shown in Figure 2a.

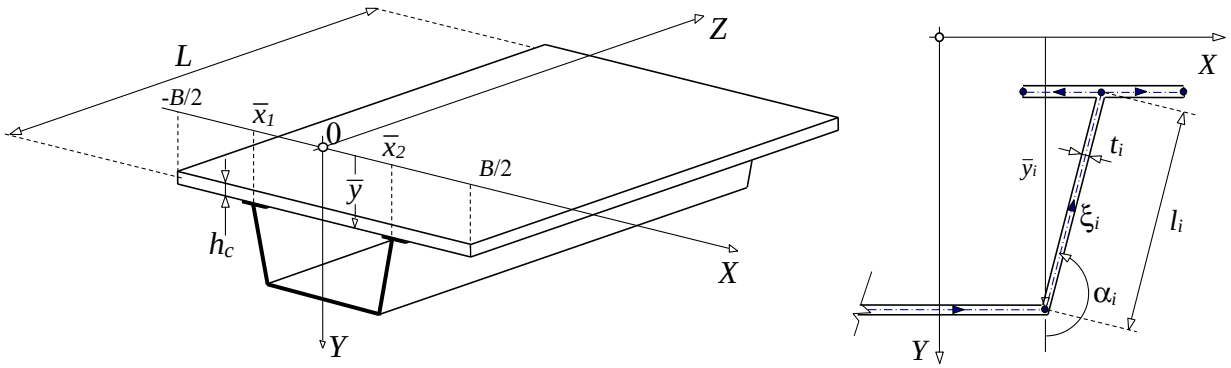

(**a**) (**b**)

Figure 2. (**a**) Cross-section geometry; (**b**) local abscissa of the i-th wall.

The steel element, because of its peculiar dimensions, is assumed to be a thin-walled beam composed by n plane walls; for the i-th wall, with constant thickness t_i and length l_i, the local abscissa $\xi_i \in [0,\ l_i]$ is introduced, assuming α_i to be the direction cosine of the local abscissa with respect to the Y axis (Figure 2b).

2.1. Kinematics

The beam kinematics is characterised by null displacements in the X direction, namely the beam transverse bending and torsion are not included in the model. Furthermore, the slab–girder detachment is considered to be prevented by the shear connection, which is assumed to be stiff in the vertical direction. The displacement field of the composite beam is approximated by superimposing warping components, due to shear flows in the elements, to the overall longitudinal displacements and bending rotations [30].

With reference to the cross section of Figure 2a, adopting subscripts c, s, and r for referring to the concrete slab, the steel girder, and the slab reinforcements, respectively, the following admissible displacement field is considered:

$$w_c(x,y,z) = \boldsymbol{w}_c(z)\cdot\boldsymbol{a}_c(x,y) \tag{1}$$

$$w_s(\xi_i,z) = \boldsymbol{w}_s(z)\cdot\boldsymbol{a}_s(\xi_i) \quad i = 1,\ \ldots,\ n \tag{2}$$

$$v(x,y,z) = v_0(z) \tag{3}$$

where w_c is the longitudinal displacement of the slab and the included steel reinforcements (steel–concrete perfect bond assumption), w_s is the longitudinal displacement of the steel girder, and v_0 is the axis deflection. Furthermore,

$$\boldsymbol{w}_c^T(z) = \left[\ w_{c0}(z) \quad \Phi_c(z) \quad f_c(z)\ \right] \tag{4}$$

$$\boldsymbol{w}_s^T(z) = \left[\ w_{s0}(z) \quad \Phi_s(z) \quad f_{sv}(z) \quad f_{sh}(z)\ \right] \tag{5}$$

are vectors grouping together the generalized longitudinal displacements w_{c0} and w_{s0} measured at the origin of the Z axis, the rotation Φ_c and Φ_s with respect of the X axis, the slab warping intensity f_c, and the steel girder warping intensities f_{sv} and f_{sh}. Furthermore,

$$\boldsymbol{a}_c^T(x,y) = \left[\ 1 \quad y \quad \psi_c(x)\ \right] \tag{6}$$

$$\boldsymbol{a}_s^T(\xi_i) = \left[\ 1 \quad y(\xi_i) \quad \psi_{sv}(\xi_i) \quad \psi_{sh}(\xi_i)\ \right] \tag{7}$$

appearing in Equations (1) and (2), are geometric vectors in which ψ_c is a known warping function of the concrete slab, which is assumed to be constant within the thickness, and ψ_{sv} and ψ_{sh} are the known steel girder warping functions. Slab and steel girder warping functions are derived through the procedure proposed by Dezi et al. [24], assuming each member as a thin-walled element separated from the others and subjected to self-equilibrated elementary loading schemes of pure shear and longitudinal constant flow at the shear connection. Finally, from Equations (1) and (2), the slab–steel girder interface slip may be readily obtained as follows:

$$\Gamma(z) = \boldsymbol{w}_s\cdot\overline{\boldsymbol{a}}_s - \boldsymbol{w}_c\cdot\overline{\boldsymbol{a}}_c \tag{8}$$

where the symbol $\overline{\bullet}$ denotes quantities calculated at the interface.

2.2. Active Stress Field

A linear elastic behaviour is assumed for materials in both tension and compression (uncracked concrete under tensile stress). E_α, ν_α, and $G_\alpha = E_\alpha/2(1+\nu_\alpha)$ are the relevant Young, Poisson, and shear moduli of materials ($\alpha = c,s,r$), while ρ is the stiffness per unit length of the slab–steel girder connection.

According to the linear theory, the admissible displacement field defined by Equations (1)–(3) leads to the following relationships between stresses and overall displacements:

$$\sigma_{cz}(x,y,z) = E_c\ \left(\boldsymbol{w}_c'\cdot\boldsymbol{a}_c - \bar{\varepsilon}_{cz}\right) \quad \tau_{cxz}(x,y,z) = G_c\ \left(\boldsymbol{w}_c\cdot\boldsymbol{a}_{c,x}\right) \tag{9}$$

$$\tau_{cyz}(x,y,z) = G_c\ \left(\boldsymbol{w}_c\cdot\boldsymbol{a}_{c,y} + v_0'\right) \quad \sigma_{sz}(\xi_i,z) = \mathrm{E_s}\ \left(\boldsymbol{w}_s'\cdot\boldsymbol{a}_s - \bar{\varepsilon}_{sz}\right) \tag{10}$$

$$\tau_{s\xi z}(\xi_i,z) = \mathrm{G_s}\ \left(\boldsymbol{w}_s\cdot\boldsymbol{a}_{s,\xi} + v_0'\ \alpha_i\right) \quad \sigma_{rz}(x,y,z) = E_r\ \left(\boldsymbol{w}_c'\cdot\boldsymbol{a}_c - \bar{\varepsilon}_{rz}\right) \tag{11}$$

where $\sigma_{\alpha z}$ ($\alpha = c,s,r$) are the longitudinal normal stresses; τ_{cxz} and τ_{cyz} are the slab shear stresses on XZ and YZ planes, respectively; and $\tau_{s\xi z}$ is the steel girder shear stress in the plane of the i-th wall. In Equations (9)–(11), primes denote total derivatives with respect to z, whereas commas denote partial derivatives. Furthermore, term $\bar{\varepsilon}_{\alpha z}$ ($\alpha = c,s,r$) in

Equations (9)–(11) are stress-independent strains that may represent thermal, concrete slab shrinkage, or wire pre-stressing; these are defined as

$$\overline{\varepsilon}_{\alpha z} = \overline{\boldsymbol{\varepsilon}}_{\alpha} \cdot \boldsymbol{a}_c = \begin{bmatrix} \epsilon_{\alpha z} \\ \kappa_{\alpha x} \\ \mu_{\alpha z} \end{bmatrix} \cdot \boldsymbol{a}_c \qquad \alpha = c, r \tag{12}$$

$$\overline{\varepsilon}_{sz} = \overline{\boldsymbol{\varepsilon}}_{s} \cdot \boldsymbol{a}_s = \begin{bmatrix} \epsilon_{sz} \\ \kappa_{sx} \\ \mu_{sv} \\ \mu_{sh} \end{bmatrix} \cdot \boldsymbol{a}_s \tag{13}$$

where ϵ, κ, and μ are overall stress-independent longitudinal strains given by

$$\overline{\boldsymbol{\varepsilon}}_{\alpha} = \boldsymbol{I}_{\alpha}^{-1} \int_{A_\alpha} \widetilde{\varepsilon}_{\alpha} \boldsymbol{a}_{\alpha} \, dA \qquad \alpha = c, r \tag{14}$$

$$\overline{\boldsymbol{\varepsilon}}_{s} = \boldsymbol{I}_{s}^{-1} \sum_{i=1}^{n} t_i \int_0^{l_i} \widetilde{\varepsilon}_{s} \boldsymbol{a}_{s} \, d\xi_i \tag{15}$$

in which $\widetilde{\varepsilon}_c$, $\widetilde{\varepsilon}_r$, and $\widetilde{\varepsilon}_s$ are generic nonlinear stress-independent longitudinal strain fields in concrete, reinforcements, and structural steel, respectively. $\boldsymbol{I}_\alpha$ and $\boldsymbol{I}_s$ appearing in Equations (14)–(15) are inertia terms of the cross section of the beam components, as detailed in Appendix A. It is worth mentioning that active stresses of Equations (9)–(11), i.e., relevant to strains descending from the admissible displacement field according to constitutive relationships, do not satisfy the local equilibrium, which also requires additional non-vanishing stress components, called reactive stresses. The latter do not appear in the virtual work theorem expression and can be estimated by means of the local equilibrium conditions. These components are significant in the case of shear stresses, while normal stresses can be obtained with negligible errors from Equations (9)–(11). Expressions of the total shear stresses τ_{cxz} and $\tau_{s\xi z}$ are available in Appendix B.

2.3. Balance Conditions

The weak form of the equilibrium conditions is derived by means of the virtual work theorem by considering the displacement field previously introduced and the constitutive laws (9)–(11) (Appendix A). By grouping the generalized displacements in the vector,

$$\boldsymbol{d}^T = \begin{bmatrix} w_{c0} & \Phi_c & f_c & w_{s0} & \Phi_s & f_{sv} & f_{sh} & v_0 \end{bmatrix} \tag{16}$$

the following equilibrium conditions in weak form can be obtained:

$$\int_0^L [\boldsymbol{K} \, \mathcal{D}\boldsymbol{d} - \overline{\boldsymbol{n}}] \cdot \mathcal{D}\hat{\boldsymbol{d}} \, dz = \int_0^L \boldsymbol{p} \cdot \hat{\boldsymbol{d}} \, dz + \left(\boldsymbol{P}_\alpha \cdot \hat{\boldsymbol{d}} \right)\big|_{\alpha=0,L} \qquad \forall \hat{\boldsymbol{d}} \neq \boldsymbol{0} \tag{17}$$

where $\hat{\boldsymbol{d}}$ is the variation of the displacement field and $\mathcal{D}$ is a formal linear differential operator defined as

$$\mathcal{D}\boldsymbol{d}(z) = \begin{bmatrix} \boldsymbol{d} \\ \boldsymbol{d}' \end{bmatrix} \tag{18}$$

In Equation (17),

$$\boldsymbol{K}(z) = \begin{bmatrix} \boldsymbol{K}_{1,1} & \boldsymbol{K}_{1,2} \\ \boldsymbol{K}_{2,1} & \boldsymbol{K}_{2,2} \end{bmatrix} = \left[\begin{array}{ccc:ccc} G_c\,\boldsymbol{J}_c + \rho\,\boldsymbol{A}_{cc} & -\rho\,\boldsymbol{A}_{cs} & \boldsymbol{0} & \boldsymbol{0} & \boldsymbol{0} & G_c\,\boldsymbol{L}_c \\ -\rho\,\boldsymbol{A}_{sc} & G_s\,\boldsymbol{J}_s + \rho\,\boldsymbol{A}_{ss} & \boldsymbol{0} & \boldsymbol{0} & \boldsymbol{0} & G_s\,\boldsymbol{L}_s \\ \boldsymbol{0} & \boldsymbol{0} & 0 & \boldsymbol{0} & \boldsymbol{0} & 0 \\ \boldsymbol{0} & \boldsymbol{0} & \boldsymbol{0} & E_c\,\boldsymbol{I}_c + E_r\,\boldsymbol{I}_r & \boldsymbol{0} & \boldsymbol{0} \\ \hdashline \boldsymbol{0} & \boldsymbol{0} & \boldsymbol{0} & \boldsymbol{0} & E_s\,\boldsymbol{I}_s & \boldsymbol{0} \\ G_c\,\boldsymbol{L}_c^T & G_s\,\boldsymbol{L}_s^T & 0 & \boldsymbol{0} & \boldsymbol{0} & G_c\,A_c + G_s\,m_s \end{array}\right] \tag{19}$$

is a matrix that contains inertia terms of the cross section of the beam components and those due to the interface connection (Appendix A). Furthermore,

$$\boldsymbol{p}^T(z) = \begin{bmatrix} q_{cz} & m_{cx} & \omega_{cy} & q_{sz} & m_{sx} & \omega_{sy} & \omega_{sx} & q_y \end{bmatrix} \tag{20}$$

$$\boldsymbol{P}_{\alpha}^T = \begin{bmatrix} N_{cz\alpha} & M_{cx\alpha} & W_{cy\alpha} & N_{sz\alpha} & M_{sx\alpha} & W_{sy\alpha} & W_{sx\alpha} & Q_{y\alpha} \end{bmatrix} \tag{21}$$

are the vectors grouping resultants of the external forces along the beam axis and at the beam end cross sections. In detail, the above vectors contain longitudinal forces (q and N), bending moments (m and M), bi-moments (ω and W), and vertical loads (q and Q). Finally, in Equation (17),

$$\overline{\boldsymbol{n}}(z,t) = \begin{bmatrix} \overline{\boldsymbol{n}}_1 \\ \overline{\boldsymbol{n}}_2 \end{bmatrix} = \left[\begin{array}{c} \boldsymbol{0} \\ \boldsymbol{0} \\ 0 \\ \hdashline E_c\boldsymbol{I}_c\overline{\boldsymbol{\varepsilon}}_c + E_r\boldsymbol{I}_r\overline{\boldsymbol{\varepsilon}}_r \\ E_s\boldsymbol{I}_s\overline{\boldsymbol{\varepsilon}}_s \\ 0 \end{array}\right] \tag{22}$$

is the vector grouping resultants of stresses due to the restrained stress-independent strains. By integrating parts and considering the fundamental theorem of variational calculus, the following strong form of the equilibrium conditions can be obtained:

$$-\boldsymbol{K}_{2,2}\boldsymbol{d}'' + (\boldsymbol{K}_{1,2} - \boldsymbol{K}_{2,1})\boldsymbol{d}' + \boldsymbol{K}_{1,1}\boldsymbol{d} = \boldsymbol{p} - \overline{\boldsymbol{n}}_2' \tag{23}$$

with the relevant boundary conditions

$$\left[-\boldsymbol{K}_{2,1}\boldsymbol{d} - \boldsymbol{K}_{2,2}\boldsymbol{d}' + \overline{\boldsymbol{n}}_2 - \boldsymbol{P}_0\right]\cdot\hat{\boldsymbol{d}}\big|_0 = \boldsymbol{0} \quad \forall\hat{\boldsymbol{d}} \tag{24}$$

$$\left[\boldsymbol{K}_{2,1}\boldsymbol{d} + \boldsymbol{K}_{2,2}\,\boldsymbol{d}' - \overline{\boldsymbol{n}}_2 - \boldsymbol{P}_L\right]\cdot\hat{\boldsymbol{d}}\big|_L = \boldsymbol{0} \quad \forall\hat{\boldsymbol{d}} \tag{25}$$

2.4. Analytical Solution

The strong form of equilibrium condition (23) has been used by Gara et al. [30] to obtain a closed form solution of the problem, exploiting properties of exponential matrices. This approach has the advantage of avoiding a spatial discretization, but may lead to instabilities due to the numerical computation of the exponential matrix in the case of long beams. The procedure is herein recalled because it will be later exploited to develop one of the proposed finite elements.

By defining $\boldsymbol{s}(z) = \mathcal{D}\boldsymbol{d}$, Equations (23)–(25) can be rewritten in the canonical form

$$\boldsymbol{s}' - \boldsymbol{B}\boldsymbol{s} = \boldsymbol{c} \tag{26}$$

$$\left[-\boldsymbol{C}\,\boldsymbol{s} + \overline{\boldsymbol{n}}_2 - \boldsymbol{P}_0\right]\cdot\hat{\boldsymbol{d}}\big|_0 = \boldsymbol{0} \quad \forall\hat{\boldsymbol{d}} \tag{27}$$

$$\left[\boldsymbol{C}\,\boldsymbol{s} - \overline{\boldsymbol{n}}_2 - \boldsymbol{P}_L\right]\cdot\hat{\boldsymbol{d}}\big|_L = \boldsymbol{0} \quad \forall\hat{\boldsymbol{d}} \tag{28}$$

where

$$\boldsymbol{B}(z) = \begin{bmatrix} \mathbf{0} & \boldsymbol{I} \\ \boldsymbol{K}_{2,2}^{-1}\boldsymbol{K}_{1,1} & \boldsymbol{K}_{2,2}^{-1}(\boldsymbol{K}_{1,2} - \boldsymbol{K}_{2,1}) \end{bmatrix} \tag{29}$$

and

$$\boldsymbol{C}(z) = \begin{bmatrix} \boldsymbol{K}_{2,1} & \boldsymbol{K}_{2,2} \end{bmatrix} \tag{30}$$

are matrices containing stiffness terms of the composite beam cross section and

$$\boldsymbol{c}(z) = \begin{bmatrix} \mathbf{0} \\ -\boldsymbol{K}_{2,2}^{-1}\,(\boldsymbol{p} - \overline{\boldsymbol{n}}_2') \end{bmatrix} \tag{31}$$

is a vector depending on loads and stress-independent strains distributed along the beam axis. Equation (26) is a linear system of ordinary differential equations with constant coefficients having the solution

$$\boldsymbol{s} = \boldsymbol{E}(z)\,\boldsymbol{b} + \boldsymbol{E}(z)\int \boldsymbol{E}(z)^{-1}\,\boldsymbol{c}(z)\,dz \tag{32}$$

obtained by summing the complementary solution (i.e., of the homogeneous problem) to a particular one of the non-homogeneous problem. In Equation (32), $\boldsymbol{E}$ is the exponential matrix defined by the series expansion

$$\boldsymbol{E}(z) = \sum_{k=0}^{\infty} \frac{1}{k!}\boldsymbol{B}^k z^k \tag{33}$$

and $\boldsymbol{b}$ is the vector of the integration constants obtained by imposing boundary conditions. The derivations of displacements relevant to beams with imposed end displacements (homogenous problem with non-homogenous boundary conditions) and beams with clamped ends subjected to distributed loads (non-homogenous problem with homogenous boundary conditions) will be necessary in the next section and are provided below.

2.4.1. Beam with Imposed End Displacements

The case of an unloaded beam with non-homogeneous boundary conditions is representative of a composite beam subjected to generic end displacements. By setting $\boldsymbol{c} = \mathbf{0}$ and assuming that $\boldsymbol{u}_0$ and $\boldsymbol{u}_L$ are the known beam end-displacements, Equation (32) yields

$$\boldsymbol{s}_h(z) = \boldsymbol{E}(z)\boldsymbol{R}\boldsymbol{U} \tag{34}$$

in which

$$\boldsymbol{R} = \begin{bmatrix} \cup\,\boldsymbol{E}(0) \\ \cup\,\boldsymbol{E}(L) \end{bmatrix}^{-1} \qquad \boldsymbol{U} = \begin{bmatrix} \boldsymbol{u}_0 \\ \boldsymbol{u}_L \end{bmatrix} \tag{35}$$

2.4.2. Beam with Distributed Loads

The case of a beam subjected to distributed loads with homogeneous boundary conditions ($\boldsymbol{U} = \mathbf{0}$) is representative of a beam with fixed ends. For the sake of simplicity, a linearly distributed load $\boldsymbol{c}(z) = \boldsymbol{c}_0 + \boldsymbol{c}_1 z$ along the axis is considered. Considering the following properties of the exponential matrix:

$$\int \boldsymbol{E}^{-1}dz = -\boldsymbol{B}^{-1}\boldsymbol{E}^{-1} \qquad \int \boldsymbol{E}^{-1}\,z\,dz = -(\boldsymbol{B}^{-1})^2\boldsymbol{E}^{-1}(\boldsymbol{B}z + \boldsymbol{I}) \tag{36}$$

after some manipulations, Equation (32) yields

$$\boldsymbol{s}_p(z) = \boldsymbol{E}\,(\boldsymbol{R}\,\boldsymbol{Q}_0\boldsymbol{c}_0 + \boldsymbol{R}\,\boldsymbol{Q}_1\boldsymbol{c}_1) - \boldsymbol{E}\boldsymbol{B}^{-1}\boldsymbol{E}^{-1}\boldsymbol{c}_0 - \boldsymbol{E}(\boldsymbol{B}^{-1})^2\boldsymbol{E}^{-1}(\boldsymbol{B}z + \boldsymbol{I})\boldsymbol{c}_1 \tag{37}$$

where

$$\boldsymbol{Q}_0 = \begin{bmatrix} \cup\,(\boldsymbol{E}(0)\boldsymbol{B}^{-1}\boldsymbol{E}(0)^{-1}) \\ \cup\,(\boldsymbol{E}(L)\boldsymbol{B}^{-1}\boldsymbol{E}(L)^{-1}) \end{bmatrix} \tag{38}$$

$$\boldsymbol{Q}_1 = \begin{bmatrix} \cup\,(\boldsymbol{E}(0)(\boldsymbol{B}^{-1})^2\boldsymbol{E}(0)^{-1}) \\ \cup\,(\boldsymbol{E}(L)(\boldsymbol{B}^{-1})^2\boldsymbol{E}(L)^{-1}(\boldsymbol{B}L+\boldsymbol{I})) \end{bmatrix} \tag{39}$$

3. Proposed Higher Order Finite Elements

As already mentioned, the closed form solution proposed in Gara et al. [30] suffers for numerical instability problems due to the computation of the exponential matrix in the case of long beams; in this case, a discretization of the beam axis is necessary to consider beam sections of reduced lengths. Furthermore, a closed form approach requires the computation of the particular solution, which depends on the specific load distribution. Finally, the beam discretization is required in the case of beams partially loaded along the axis, or in the case of beams with varying cross section properties. Consequently, a finite element approach for the problem solution, through numerical integration of the equilibrium condition in weak form (17), appears convenient considering its versatility to manage the above issues.

By dividing the beam axis into n_e finite elements, the displacement $\boldsymbol{d}(\eta)$ within the generic element may be obtained by

$$\boldsymbol{d}(\eta) \cong \boldsymbol{N}_e(\eta)\,\boldsymbol{v}_e \tag{40}$$

where η is the local abscissa, $\boldsymbol{v}_e$ is the vector of the unknown nodal displacements, and $\boldsymbol{N}_e(\eta)$ is a matrix containing known interpolating functions.

Taking into account Equation (40), the equilibrium condition (17) leads to the following global equilibrium system obtained by assembling contributions of all elements:

$$\boldsymbol{K}\,\boldsymbol{v} = \boldsymbol{f}_p + \boldsymbol{f}_{\overline{n}} \tag{41}$$

where $\boldsymbol{v}$ is the vector of nodal displacements of the whole model, suitably assembled from $\boldsymbol{v}_e$ of all the elements. In Equation (41),

$$\boldsymbol{K} = \bigwedge_{e=1}^{n_e} \int_{l_e} (\mathcal{D}\boldsymbol{N})_e^T\,\boldsymbol{K}\,\mathcal{D}\boldsymbol{N}_e\,d\eta \tag{42}$$

is the global stiffness matrix of the composite beam and

$$\boldsymbol{f}_p = \bigwedge_{e=1}^{n_e} \int_{l_e} \boldsymbol{N}_e^T\,\boldsymbol{p}\,d\eta \qquad \boldsymbol{f}_{\overline{n}} = \bigwedge_{e=1}^{n_e} \int_{l_e} (\mathcal{D}\boldsymbol{N})_e^T\,\overline{\boldsymbol{n}}\,d\eta \tag{43}$$

are nodal force vectors due to external loads and stress-independent strains, respectively, obtained by assembling the relevant matrices and vectors defined for the single finite element.

3.1. Definition of the Beam Finite Elements

In finite element applications, the solution accuracy is strongly related to the mesh of nodes where unknown displacements have to be calculated, and to the interpolating functions, which are necessary to approximate displacement fields within each element. In this paper, three types of finite elements are developed, hereafter referred to as *GFE*, *CIFE*, and *IIFE* [33], each characterised by different interpolating functions.

3.1.1. Linear Interpolating Functions

The *GFE* adopts linear interpolating functions for the displacements, resulting in a 16-dof higher order composite beam finite element (Figure 3). The vector of nodal displacements is

$$\boldsymbol{v}_e^T = \left[\; w_{c01},\; \Phi_{c1}, f_{c1}, w_{s01}, \Phi_{s1}, f_{sv1}, f_{sh1},\; v_{01},\; w_{c02},\; \Phi_{c2}, f_{c2}, w_{s02}, \Phi_{s2}, f_{sv2}, f_{sh2},\; v_{02} \; \right] \tag{44}$$

and the interpolating functions matrix is

$$\boldsymbol{N}_e = \left[\; \mu \boldsymbol{I}_{7\times 7} \quad \lambda \boldsymbol{I}_{7\times 7} \; \right] \tag{45}$$

where $I_{7\times 7}$ is the identity matrix of dimension 7 and

$$\mu = 1 - \frac{\eta}{l_e} \qquad \lambda = \frac{\eta}{l_e} \tag{46}$$

are the linear interpolating functions in which η is the longitudinal abscissa of the finite element of length l_e.

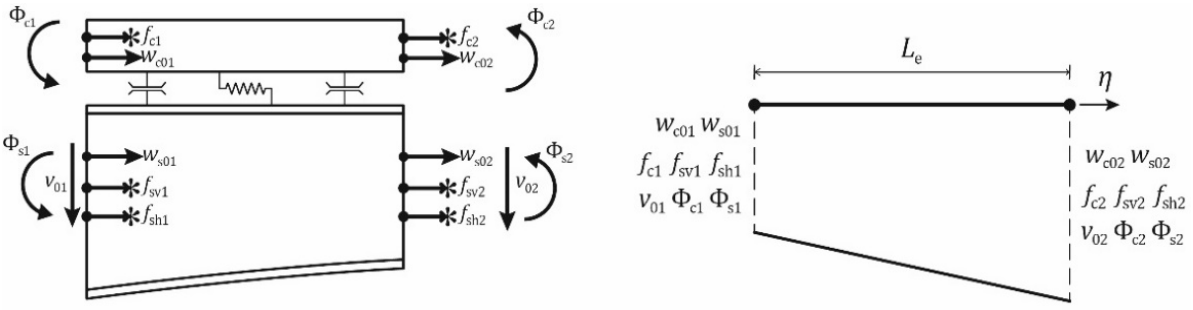

Figure 3. (**a**) Nodal generalized displacements of the general finite element *(GFE)*, (**b**) interpolation along its abscissa.

3.1.2. Polynomial Interpolating Functions

The *CIFE* implements polynomial functions of suitable orders to avoid locking problems; this is achieved by adopting interpolating functions such that contributions to deformation, due to each nodal displacement, are approximated by polynomials of the same degree. Second order Hermitian polynomials can be used for longitudinal displacements, rotations, and warping intensities by adding an intermediate node, while third-order polynomials are used for vertical displacements (Figure 4). This implies a 25-dof finite element characterised by the nodal displacements vector

$$\begin{aligned} \boldsymbol{v}_e^T = [&w_{c01},\; \Phi_{c1}, f_{c1}, w_{s01}, \Phi_{s1}, f_{sv1}, f_{sh1},\; v_{01},\; w_{c02}, \Phi_{c2}, f_{c2}, w_{s02}, \Phi_{s2}, f_{sv2}, f_{sh2},\; v_{02}, \\ &w_{c03},\; \Phi_{c3}, f_{c3}, w_{s03}, \Phi_{s3}, f_{sv3}, f_{sh3},\; v'_{01}, v'_{02}] \end{aligned} \tag{47}$$

and the relevant interpolating function matrix

$$\boldsymbol{N}_e = \begin{bmatrix} \mu_1 \boldsymbol{I}_{7\times 7} & \boldsymbol{0}_{7\times 1} & \mu_2 \boldsymbol{I}_{7\times 7} & \boldsymbol{0}_{7\times 1} & \mu_3 \boldsymbol{I}_{7\times 7} & \boldsymbol{0}_{7\times 1} & \boldsymbol{0}_{7\times 1} \\ \boldsymbol{0}_{1\times 7} & \nu_1 & \boldsymbol{0}_{1\times 7} & \nu_2 & \boldsymbol{0}_{1\times 7} & \upsilon_1 & \upsilon_2 \end{bmatrix} \tag{48}$$

in which

$$\mu_1 = 2\lambda^2 - 3\lambda + 1 \qquad \mu_2 = 2\lambda^2 - \lambda \qquad \mu_3 = -4\lambda^2 + 4\lambda \tag{49}$$

$$\nu_1 = 2\lambda^3 - 3\lambda^2 + 1 \qquad \nu_2 = -2\lambda^3 + 3\lambda^2 \tag{50}$$

$$\upsilon_1 = l_e\lambda^3 - 2\, l_e\lambda^2 + l_e\lambda \qquad \upsilon_2 = l_e\lambda^3 - l_e\lambda^2 \tag{51}$$

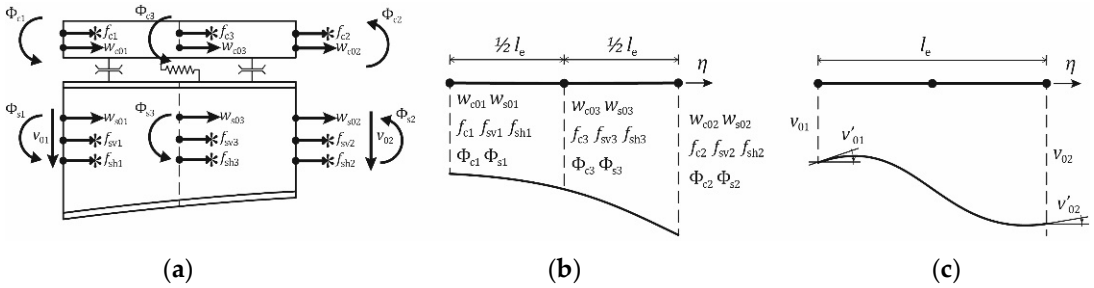

Figure 4. (**a**) Nodal generalized displacements of the consistent interpolation finite element (*CIFE*); (**b**) interpolation of longitudinal displacement, warping intensities, and rotations; and (**c**) interpolation of vertical displacement.

3.1.3. Interdependent Interpolating Functions

For the *IIFE*, nodal displacements are approximated with functions deriving from the analytical solution of the homogeneous problem of a beam subjected to generic end-displacements (34).

Considering solution (34) for the single finite element and $\boldsymbol{U} \equiv \boldsymbol{v}_e$, the interpolating functions matrix

$$\boldsymbol{N}_e(\eta) = \cup\, \boldsymbol{E}(\eta)\, \boldsymbol{R} \tag{52}$$

can be derived. The *IIFE* provides exact values of displacements for homogeneous problems, namely for beams subjected to end cross-section displacements. For non-homogeneous problems ($\boldsymbol{c} \neq \boldsymbol{0}$), the contribution of the particular integral of the analytical solution has to be added to displacements when post-processing results, according to

$$\boldsymbol{d}(\eta) = \boldsymbol{N}_e(\eta)\, \boldsymbol{d}_e + \cup\, \boldsymbol{s}_p(\eta) \tag{53}$$

where $\boldsymbol{s}_p(\eta)$ is derived by (37).

3.2. Convergence Analysis of the Proposed Finite Elements

In this section, the results of applications carried out with the proposed beam finite elements are presented and discussed to compare their rate of convergence. Analyses are performed with reference to a steel–concrete composite bridge deck with a constant box cross section, having the geometry and mechanical properties reported in Figure 5, which are representative of a concrete grade C25/30 and structural steel (European grade S). The three static schemes reported in Figure 6b are considered; *S1* is representative of single span simply supported bridge decks, while *S2* and *S3* are representative of edge and inner spans of continuous bridges, respectively. Furthermore, four loading conditions are analysed (Figure 6a); these include a uniformly distributed load (*UDL*), a concentrated load (*CL*), the concrete slab shrinkage (*SS*), and the prestressing of wires in the concrete slab (*PW*). Hereafter, analysis cases will be labelled combining the static scheme with the loading condition (e.g., *S1-UDL* refers to simply supported beam with uniformly distributed load).

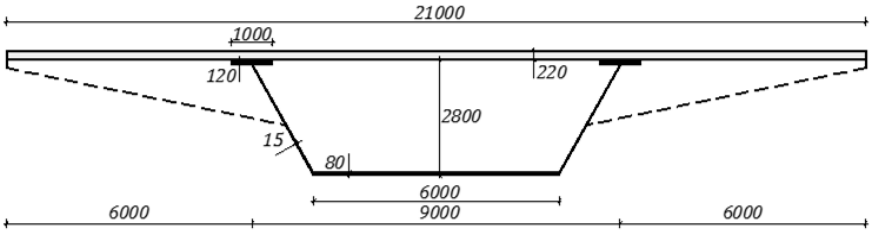

$\rho = 12000\ \mathrm{N/mm^4}$
$E_c = 31447\ \mathrm{N/mm^2}$
$E_{s,r} = 210000\ \mathrm{N/mm^2}$
$\nu_c = 0.15$
$\nu_{s,r} = 0.30$

Figure 5. Cross section adopted in the applications.

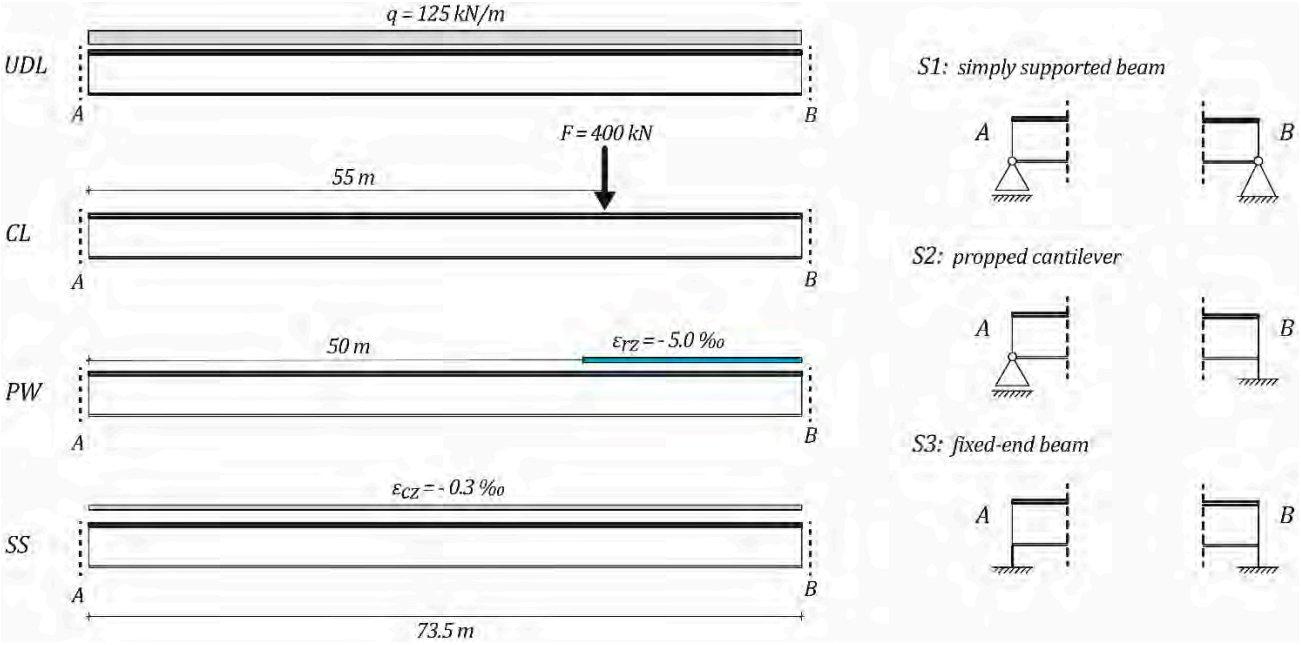

(**a**) (**b**)

Figure 6. (**a**) Load conditions and (**b**) static schemes considered in the applications. UDL, uniformly distributed load; CL, concentrated load; SS, concrete slab shrinkage; PW, prestressing of wires in the concrete slab.

The rate of convergence of models implementing the presented finite elements is analyzed by progressively increasing the number of finite elements adopted to discretize the bridge deck and by comparing the beam response with the reference one obtained considering the *IIFE* and a high number of finite elements (200 elements). For the sake of brevity, only some of the response parameters are monitored; the selected set includes displacements (vertical displacement v_0 of the composite beam, longitudinal displacement $w_{s,inf}$ of the steel girder bottom flange, warping intensity f_c), stress resultants (axial force N_c on the concrete slab, bending moment M_s on the steel girder), and the slab–girder interface slip Γ_z. Furthermore, in order to discuss the rate of convergence of the solutions, the following coefficient of variation (COV) is calculated for each response parameter by varying the beam discretization:

$$\sigma_p^* = \frac{1}{\mu_{|p|,ex}} \sqrt{\frac{1}{n} \sum_{i=1}^{n} |p_i - p_{i,ex}|^2} \tag{54}$$

where p denotes the generic response parameter, n is the number of nodes of the discretization, p_i is the value of the p-th response parameter at the i-th node, $p_{i,ex}$ is the relevant value of the reference solution (exact), and $\mu_{|p|,ex}$ is the arithmetic mean of the absolute values of the reference solution (i.e., the arithmetic mean of the absolute $p_{i,ex}$ values). The above coefficient is representative of the overall error within the beam, normalised with respect to a quantity proportional to the area of the graph of the generic response parameter.

Figure 7 plots the considered response parameters along the non-dimensional beam length z/L for case study *S2-UDL*. The results are normalised with respect to the maximum absolute value of the relevant quantity of the reference solution. In detail, Figure 7a refers to the *GFE*, while Figure 7b refers to the *CIFE*; for both cases, the results obtained by discretizing the beam length into 2, 4, 8, 16, and 50 elements are reported. The solution obtained by implementing the *IIFE* is not shown as it is almost exact, independently of the beam discretization, provided that enough elements are used to avoid computational issues in the numerical evaluation of the exponential matrix [34]. With reference to stress

resultants N_c and M_s, trends within the elements are constant and linear for the *GFE* and the *CIFE*, respectively, consistent with the adopted interpolating functions.

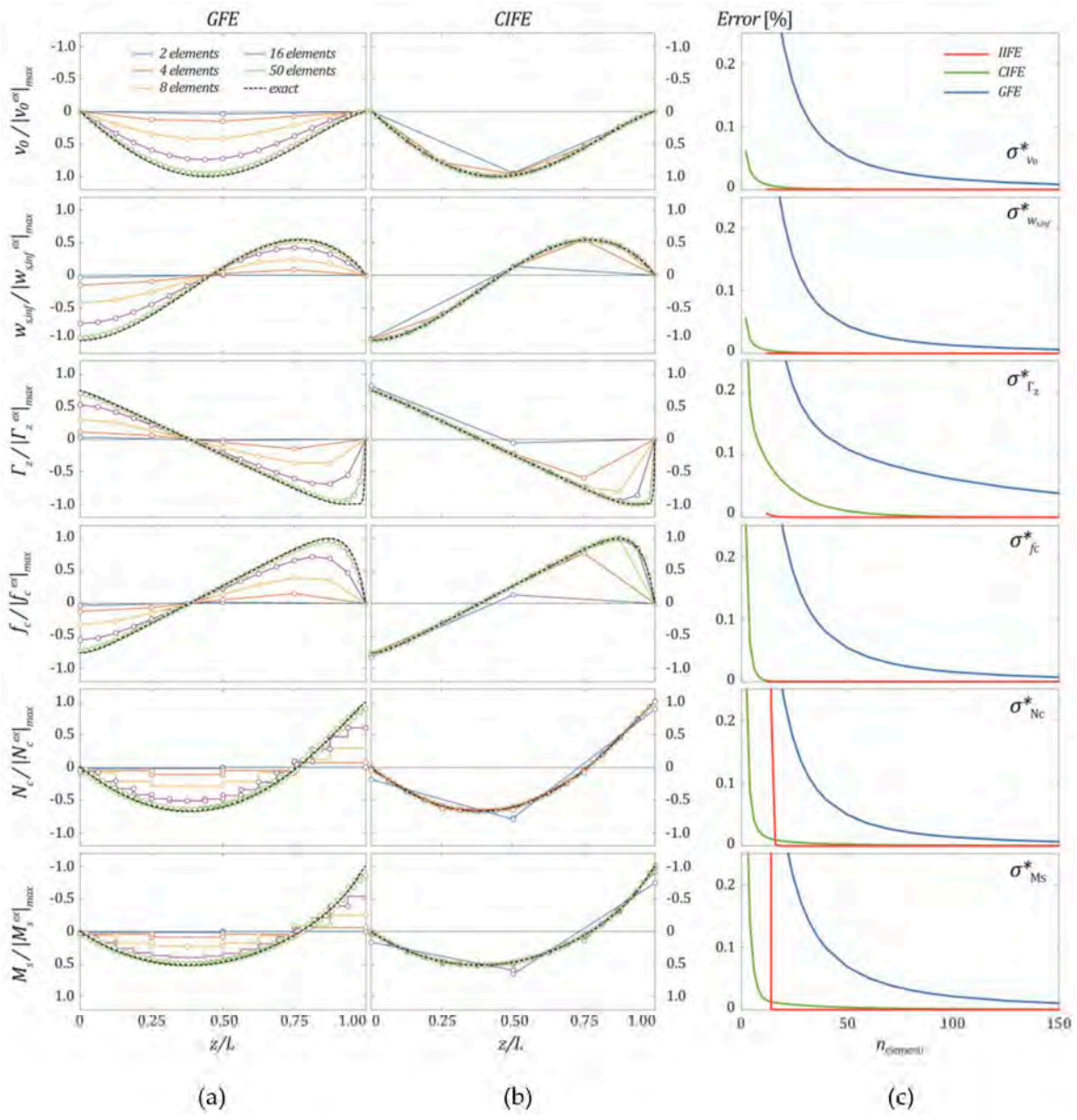

Figure 7. *S2-UDL*: Normalized beam response quantities for the (**a**) *GFE* and (**b**) *CIFE*; (**c**) errors with respect to the reference solution.

Overall, convergence for the *CIFE* is faster than that relevant to the *GFE*, especially for displacements for which good results can be obtained with very few *CIFE*s. The rate of convergence of each finite element is presented through the COV in Figure 7c as a function of the beam discretization; in this case, results considering up to 150 finite elements are shown and results relevant to the *IIFE* are addressed. The COVs confirm the faster convergence of the *CIFE* over the *GFE*, especially for displacements, and show that the slab–girder interface slip Γ_z is characterised by the lowest rate of convergence. Furthermore, overall errors lower than 5% can be achieved by using few *CIFE* (about 10, excluding Γ_z, or about 25, including Γ_z), while a higher number of *GFE*s is needed to get errors of a similar magnitude, due to locking problems (about 60, excluding Γ_z, or about 125, including Γ_z).

Finally, as already stated, the solution obtained through the *IIFE* is practically exact for the minimum number of finite elements avoiding computational issues [34]; in this framework, it is interesting to observe that, at least with reference to displacements, a sufficiently accurate solution can be obtained through *CIFE* by adopting a lower number of elements than that required to avoid computational issues. It is worth stating that the *IIFE* does not suffer for the usual higher errors in the force evaluation.

Figure 8 shows the selected normalised beam response parameters for case study *S3-CL*. Figure 8a refers to the *GFE*, while Figure 8b refers to the *CIFE*. With respect to the previous case, the number of finite elements (equal to 3, 4, 8, 16, and 51) is slightly changed for the need of applying the concentrated load. The previous considerations generally hold. COVs reported in Figure 8c once again demonstrate that the *CIFE* is overall highly competitive with respect to the *IIFE*. Figure 9, similarly to previous ones, refers to case study *S2-SS*. Discretizations involving 2, 4, 8, 16, and 50 elements are considered. Overall, the previous observation concerning the performance of the *CIFE* holds even if the *IIFE* performs better below 50 elements.

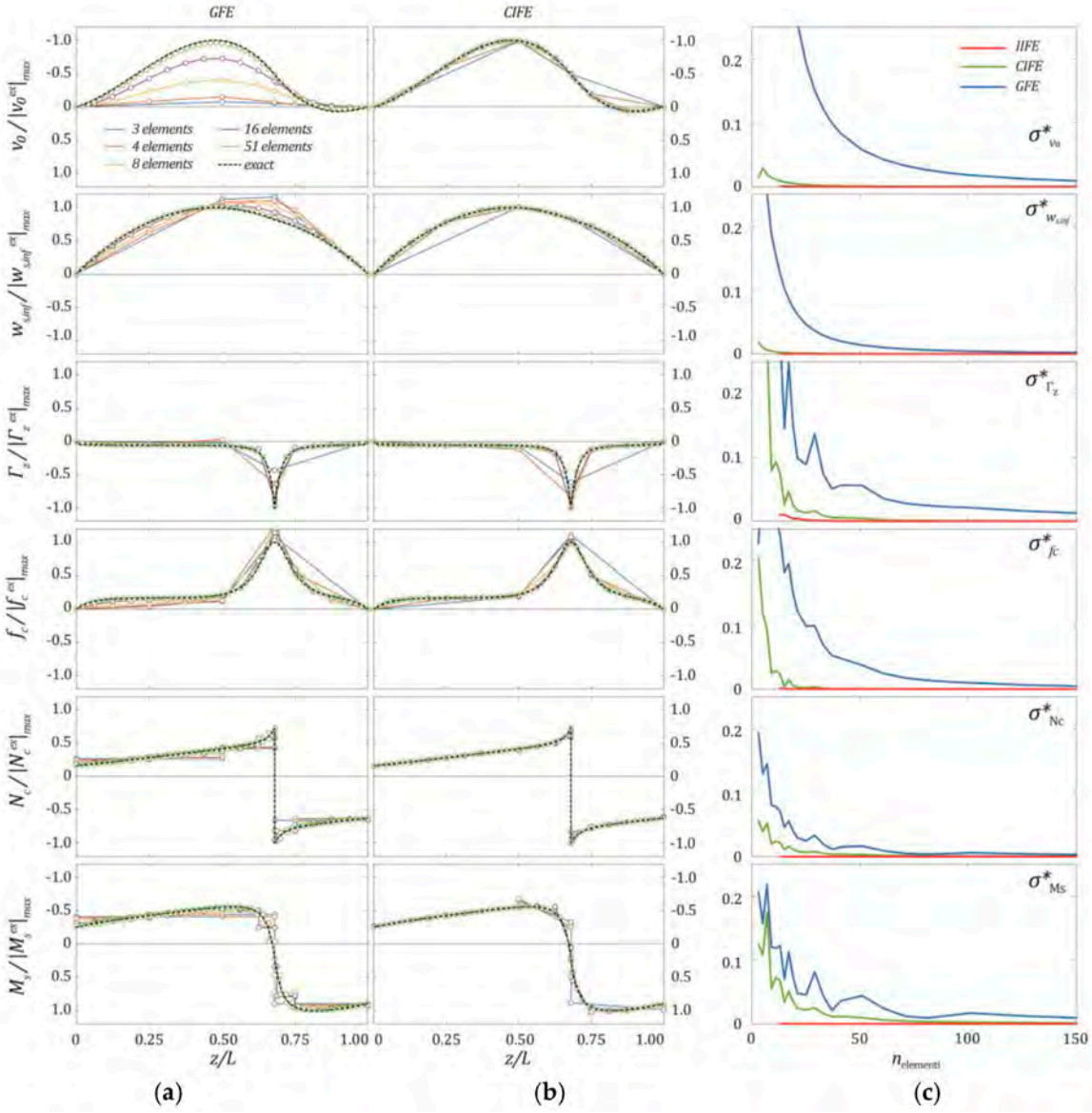

Figure 8. *S3-CL*: Normalized beam response quantities for the (**a**) *GFE* and (**b**) *CIFE*; (**c**) errors with respect to the reference solution.

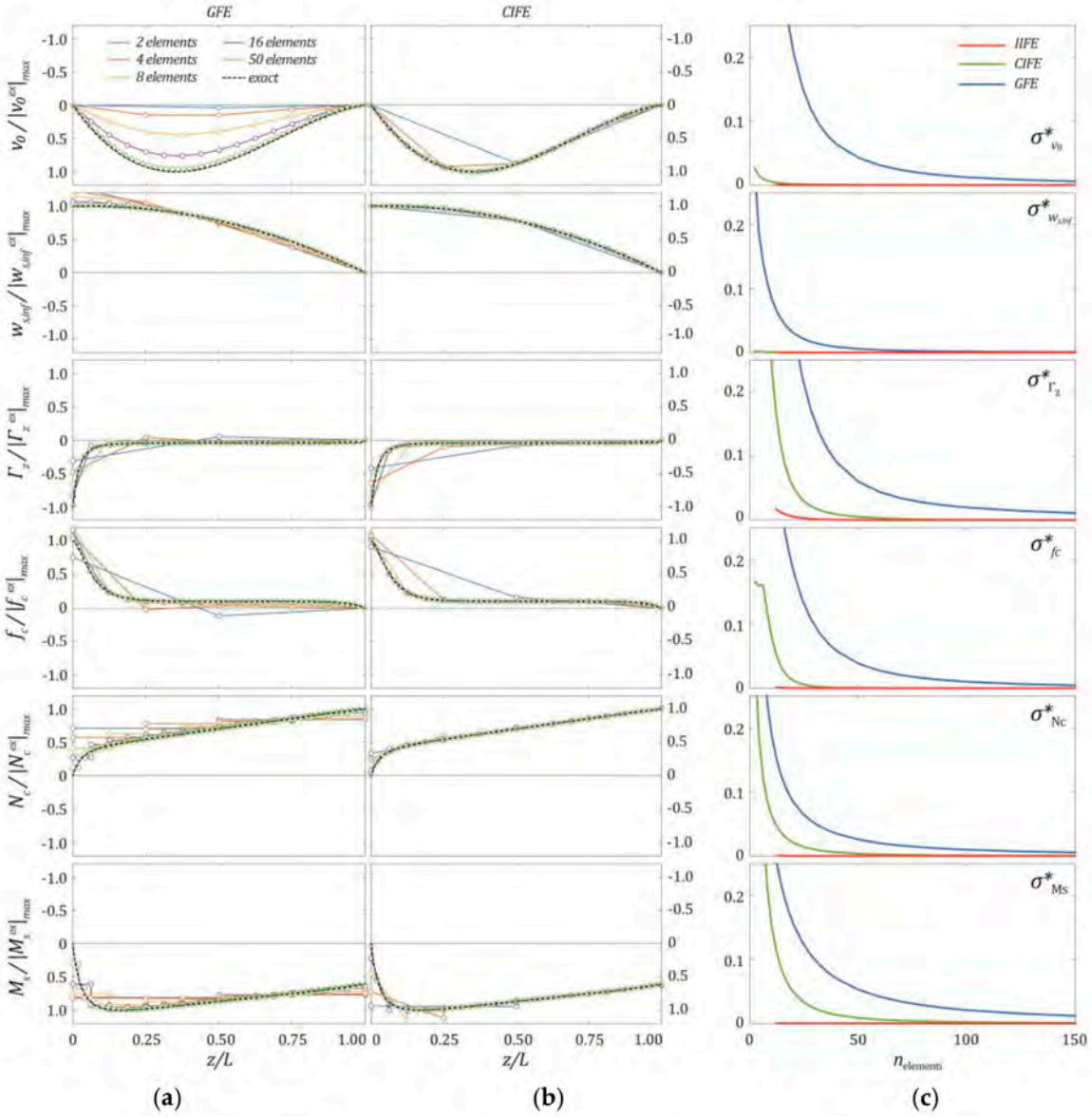

Figure 9. *S2-SS*: Normalized beam response quantities for the (**a**) *GFE* and (**b**) *CIFE*; (**c**) errors with respect to the reference solution.

Finally, Figure 10 reports the results obtained for case study *S3-PR*. It is worth stating that, in these three last cases, the convergence rate of the *GFE* and *CIFE* for forces and interface slippage is sensibly lower than that of the *IIFE*, which provides the exact solution with very few elements.

Figure 11 shows the COVs evaluated for all the case studies (derived from the combination of the static schemes with the loading conditions) and for all the kinematic response parameters. Each plot, referring to a specific case study, is further subdivided into three subplots of different colours, relevant to the results obtained considering the *GFE*, the *CIFE*, and the *IIFE*. Overall, it was found that, independent of the adopted finite element, the steel girder warping intensities (f_{sv} and f_{sh}) present higher COVs than the remaining parameters; thus, in each plot, a synthetic representation of results is proposed adopting shaded areas to trace envelops of COVs of all response parameters, excluding the steel girder warping intensities, while specific symbols are used for the latter. As expected, analyses show that the *IIFE* provides the best solution with the lower number of finite elements (i.e., the one necessary to achieve a numerical evaluation of the exponential matrix); independent of the static scheme, for both uniformly distributed (*UDL*) and concentrated loads (*CL*), about 10

elements are necessary to obtain an almost exact solution, also with reference to the steel girder warping intensities. The number of necessary finite elements rises to about 50 if wires prestressing (*PW*) or concrete shrinkage (*SS*) are considered.

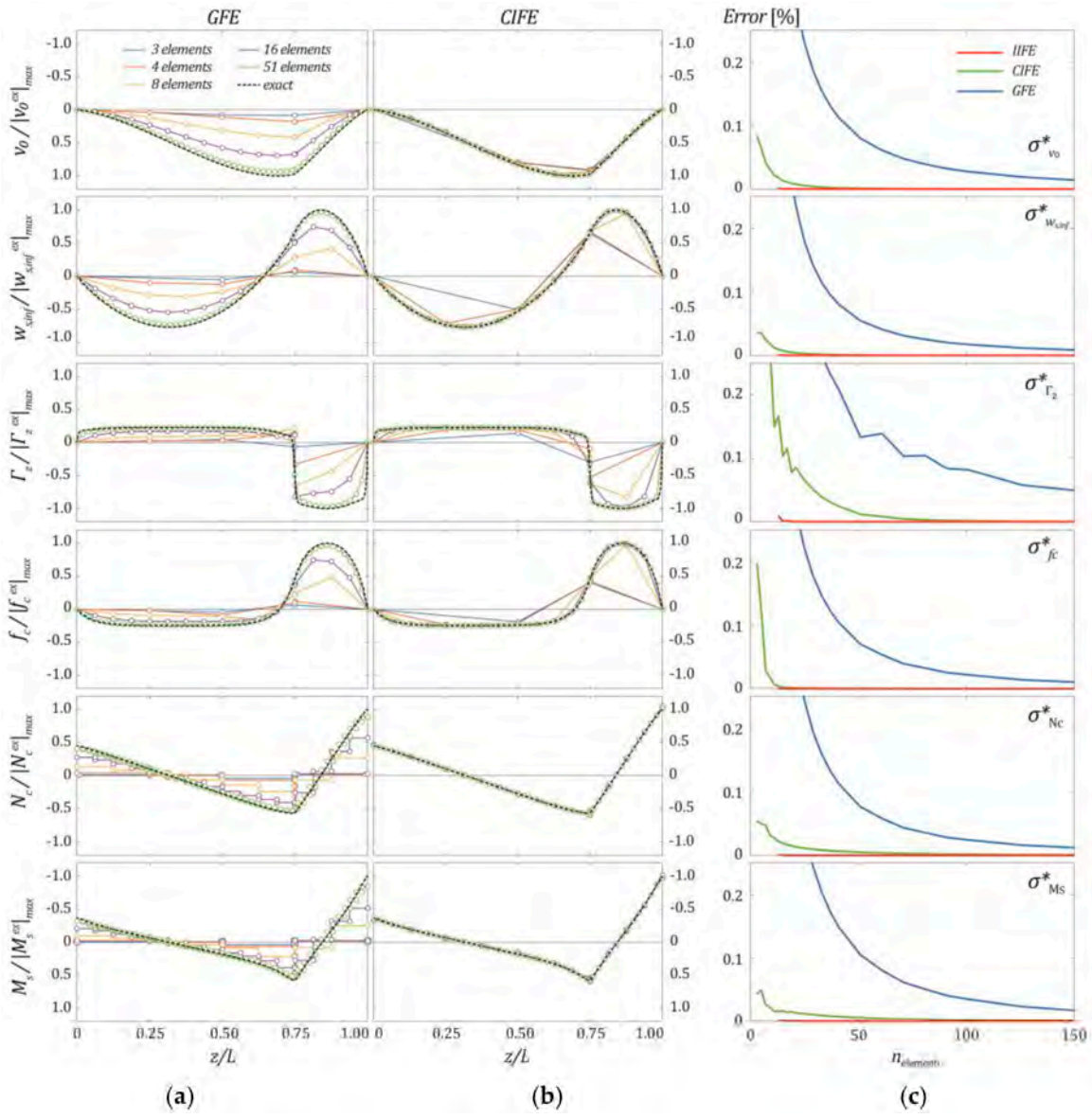

Figure 10. *S3-PR*: Normalized beam response quantities for the (**a**) *GFE* and (**b**) *CIFE*; (**c**) errors with respect to the reference solution.

The *CIFE* is overall able to assure a sufficiently accurate solution for engineering purposes with a moderate number of elements, independent of the static scheme and the load condition. Solutions with errors no greater than 5% can be obtained with about 25 elements for all the response parameters, except for the steel girder warping intensities, for which 75 elements are required.

To achieve below 1% errors, 50 elements are required for all the response parameters, except for the steel girder warping intensities, for which 100 elements are needed (in the worst case represented by the *SS* load case). Worse results are obtained with the *GFE*, which suffers from locking problems and fails to reach the exact solution even by discretizing the axis of the beam with a large number of elements.

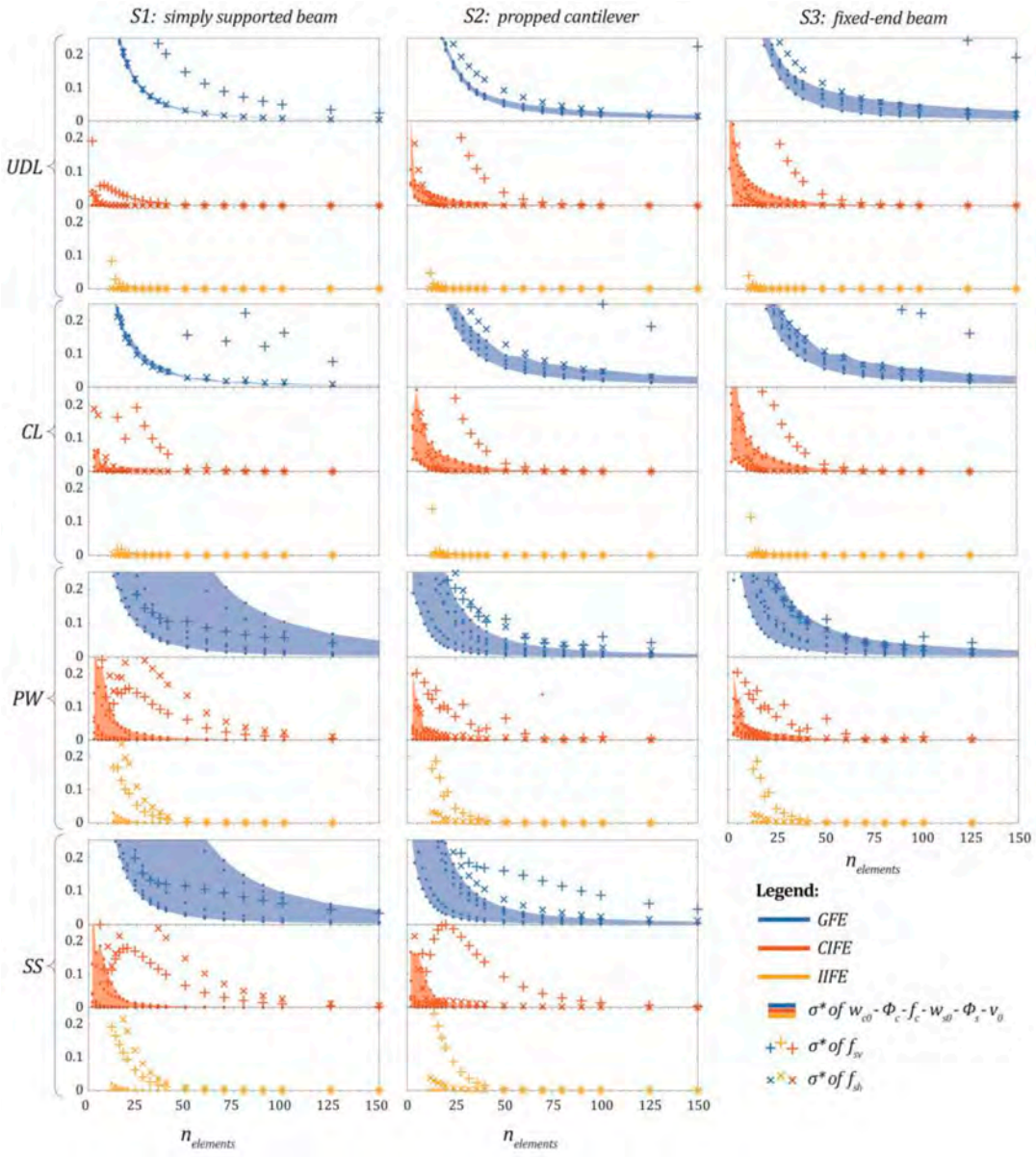

Figure 11. Trend of the coefficients of variation (COVs) for all the case studies and beam response quantities.

4. Numerical Comparison with More Complex Models

In this section, the overall efficiency of the proposed beam model in capturing the behaviour of a composite bridge deck is shown by comparing the results with those achieved with a refined three-dimensional FE model developed in SAP2000® [32]. For this purpose, all the analysis cases previously presented, including loading conditions and static schemes, are investigated.

Components of the beam cross section are modelled with four node homogenous thin shell elements that combine membrane and plate-bending behaviour and adopt a four-point numerical integration formulation. The actual position of their relevant mid planes is suitably taken into account and preliminary convergence analyses are performed on the developed FE models to define the suitable mesh dimension. In detail, the concrete slab is schematized with elements of dimensions 0.5 × 0.5 m, whereas upper flanges, webs, and bottom flanges of the steel girder are divided into 5, 6, and 12 elements, respectively.

The shear connection is modelled with two node frame elements connecting nodes of the concrete slab and the upper steel flanges, located in the relevant mid planes. Two beam

elements are adopted, pinned in correspondence of the slab–steel girder interface, having properties suitably calibrated to assure a translational stiffness equal to the one used in the previous applications. A pictorial view of the developed model is reported in Figure 12.

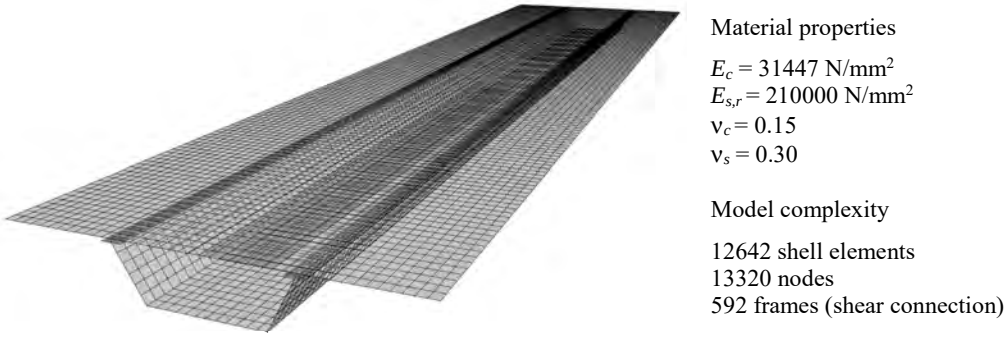

Figure 12. 3D finite element (FE) model.

Figure 13 shows the vertical deflection v_0, the slab–girder interface slip Γ_z, and the longitudinal displacements of the upper ($w_{s,sup}$) and bottom flanges ($w_{s,inf}$) of the steel girder obtained for case studies *S2-UDL*, *S3-CL*, *S2-SS*, and *S3-PW*. The results obtained considering the different beam elements (*GFE*, *CIFE*, and *IIFE*) are reported with lines of different colours and are compared with those achieved by the refined 3D FE model, represented by black dots.

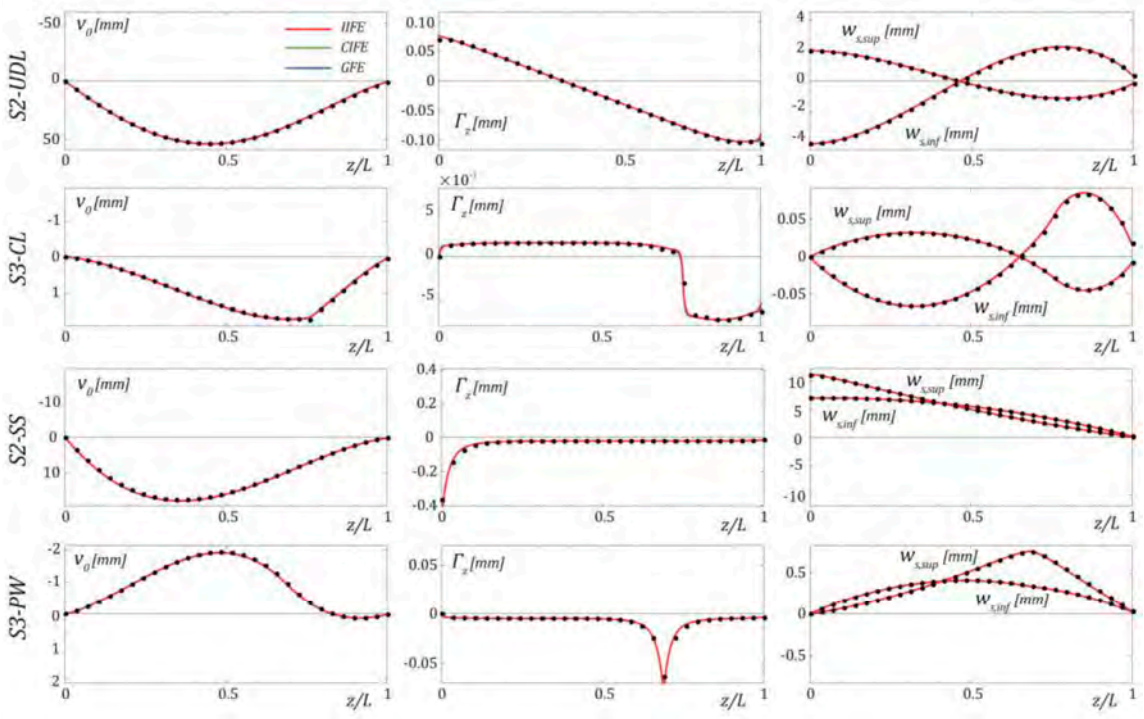

Figure 13. Comparison between the proposed beam model and the refined 3D FE model for some case studies in terms of vertical displacement v_0; interface slip Γ_z; and the longitudinal displacement of the steel girder bottom and upper flanges, $w_{s,inf}$ and $w_{s,sup}$.

Concerning the proposed beam model, a suitable number of elements is considered, on the basis of the previous applications, to assure the analysis convergence and accuracy. In detail, 200, 100, and 50 elements are considered for the *GFE*, the *CIFE*, and the *IIFE*, respectively. It can be observed that the results from the proposed beam finite elements are

practically superimposed and all perfectly match the solution achieved with the refined 3D FE model.

Figure 14 compares the normal stresses on the concrete slab mid plane, on the steel girder web, and on the steel girder bottom flange obtained from the proposed beam model with those resulting from the refined 3D FE model, for case study *S2-UDL*. As the results from the beam models are almost superimposed, for the sake of simplicity, only those relevant to the *IIFE* are reported in red. The results from the refined FE model are reported with black lines. Because the response of the slab is symmetric with respect to the longitudinal middle axis, comparisons between the beam and shell finite element models are made by dividing the plot of Figure 14a into two parts, and by presenting the distribution of stresses for half of the slab.

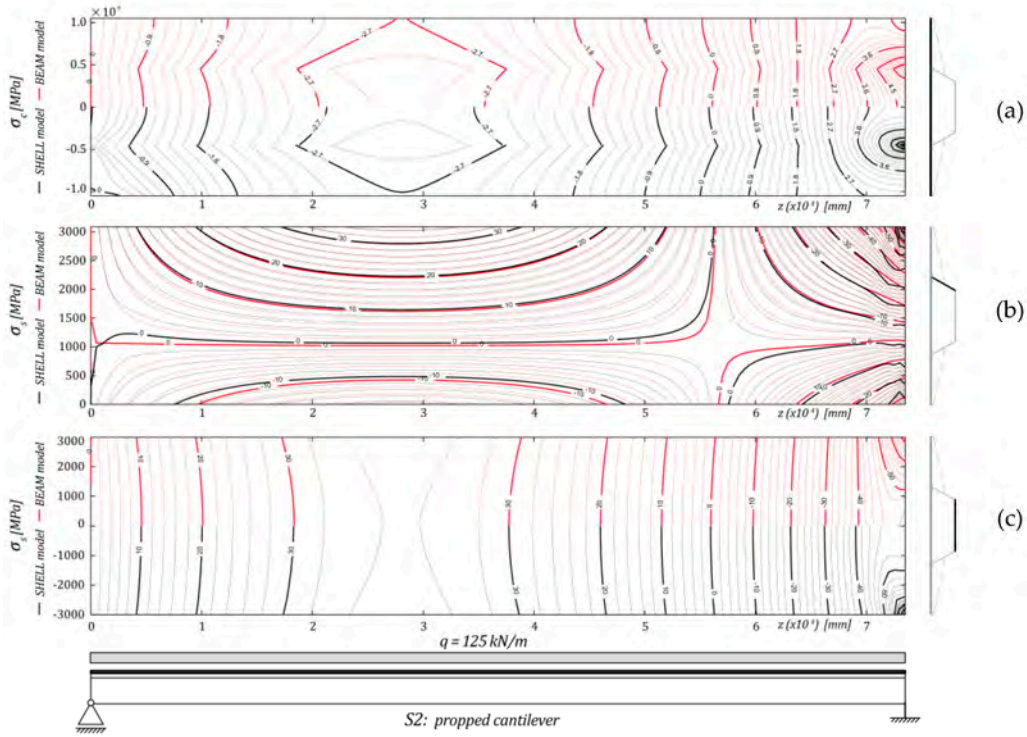

Figure 14. (**a**) Longitudinal normal stress on the slab mid plane, (**b**) on the steel girder web, and (**c**) on the steel girder bottom flange for case study *S2-UDL*.

The beam model is able to capture very well the slab normal stresses with very few differences in the bridge deck section characterised by the maximum positive bending moment and at the fixed support. Comparisons of normal stresses in the box-girder web are presented in Figure 14b by superimposing the results from the beam and shell models; normal stresses obtained by the shell model are closely reproduced with minor differences at the fixed support and in correspondence of the bridge deck section in which the overall bending moment passes from hogging to sagging. Finally, normal stresses in the bottom flange of the box-girder are compared in Figure 14c, adopting the strategy used for the concrete slab; even in this case, the beam model performs very well, furnishing results superimposed to those of the shell model.

Figure 15 compares the normal stresses on the slab mid plane, on the steel girder web, and on the steel girder bottom flange for case study *S3-CL*. As for the concrete slab (Figure 15a) and the box-girder bottom flange (Figure 15c), normal stresses of the refined shell model are closely reproduced with very small differences in the neighborhood of the applied concentrated load. Normal stresses acting on the web of the steel girder are more sensitive to the concentrated load and significant differences are observed between the proposed beam model and the refined 3D FE model (Figure 15b).

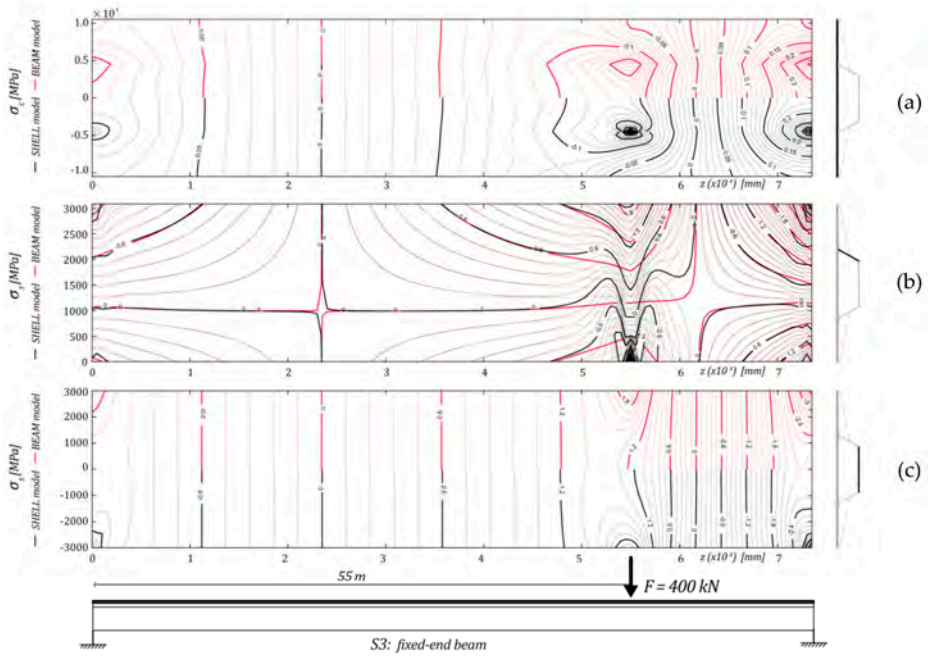

Figure 15. (**a**) Longitudinal normal stress on the slab mid plane, (**b**) on the steel girder web, and (**c**) on the steel girder bottom flange for case study *S3-CL*.

Figure 16 compares the same response parameters for case study *S2-SS*. Stresses in the concrete slab (Figure 16a) and the box-girder bottom flange (Figure 16c) resulting from the refined 3D FE model are well reproduced, with exception of only the bridge deck sections near the supports, particularly the pinned one. However, it should be remarked that stresses vanish at the pinned support, thus differences are of limited significance. Normal stresses on the web of the steel girder predicted with the proposed beam model are in very good agreement with those of the shell model, with minor discrepancies near the supports (Figure 16b).

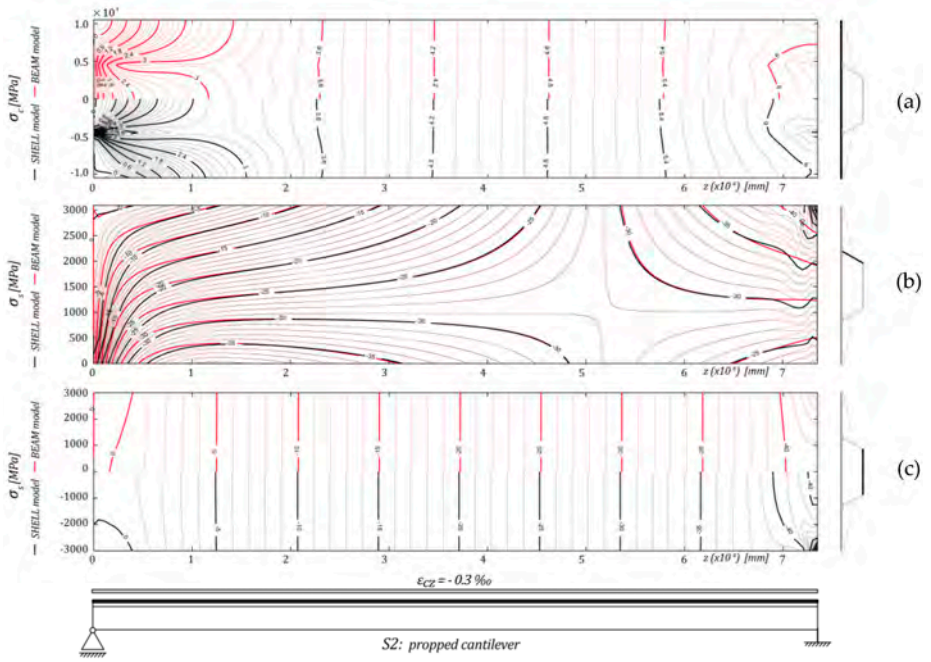

Figure 16. (**a**) Longitudinal normal stress on the slab mid plane, (**b**) on the steel girder web, and (**c**) on the steel girder bottom flange for case study *S2-SS*.

Finally, Figure 17 refers to case study *S3-PW*. Stresses in the concrete slab (Figure 17a) and the box-girder bottom flange (Figure 17c) obtained from the refined shell model are well reproduced, except for the bridge deck section subjected to the local effects induced by the pre-stressing. Normal stresses on the web of the steel girder are also well captured, even in the region affected by the pre-stressing local actions (Figure 17b).

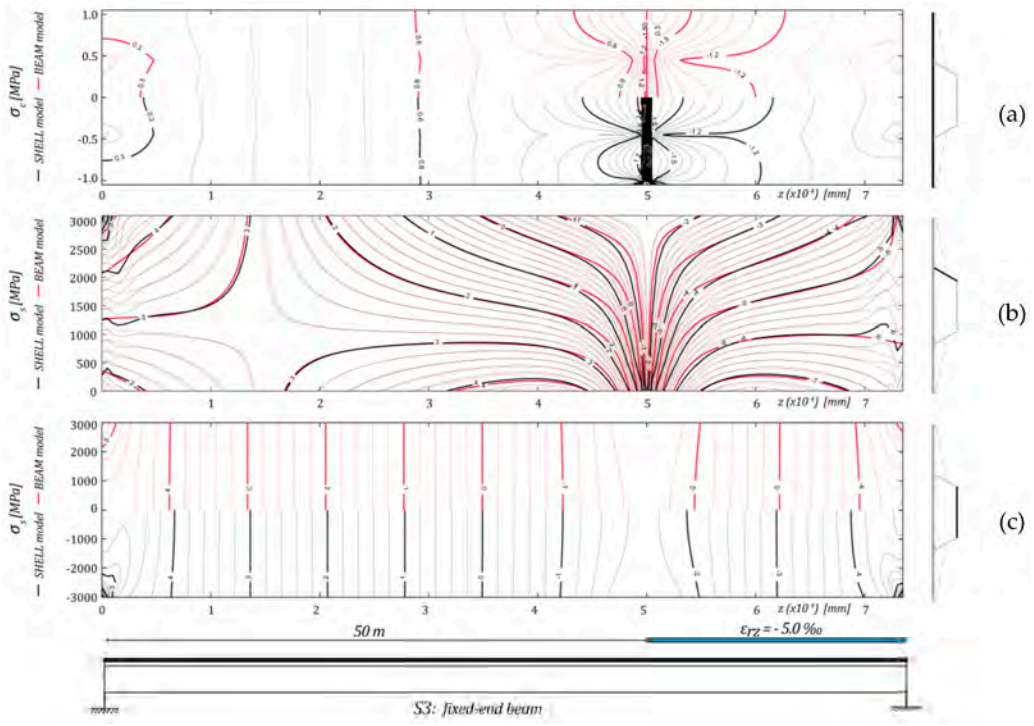

Figure 17. (**a**) Longitudinal normal stress on the slab mid plane, (**b**) on the steel girder web, and (**c**) on the steel girder bottom flange for case study *S3-PR*.

5. Conclusions

Finite elements for a higher order steel–concrete composite beam model were presented in this paper. The model, which is particularly suitable for the analysis of bridge decks, includes the partial interaction between concrete and steel members and accounts for the overall shear deformability and the shear-lag phenomenon, which strongly characterise the response of both steel and concrete elements.

Finite elements characterised by different interpolating functions are developed, implementing linear, polynomial, and exponential shape functions; the latter are derived from an analytical solution that exploits exponential matrices. The performance of the presented finite elements is investigated in terms of the solution convergence rate with reference to realistic steel–concrete composite beams with different restraints and loading conditions. The efficiency of the proposed finite elements in providing a reliable prediction of the structural response of composite beams is also addressed through comparison of the results with those achieved with a refined 3D numerical model developed using conventional shell finite elements.

The following remarks can be drawn:

- The finite element based on linear shape functions (*GFE*) suffers from locking problems and requires a highly refined discretization to reach an accurate solution of the problem;
- The finite element implementing cubic and quadratic polynomial shape functions (*CIFE*) avoids locking problems and is characterised by a higher converge rate than that based on linear shape functions (*GFE*);
- The finite element with exponential shape functions (*IIFE*) is the most performant and furnishes an almost exact solution, independent of the beam discretization, provided

that enough finite elements are adopted to avoid issues in the numerical evaluation of the exponential matrix;

- The *CIFE* is highly competitive with respect to the *IIFE*, especially in predicting beam displacements and rotations; in some cases, if very accurate solutions are not required, the former may provide results with a lower number of finite elements than that necessary to avoid instabilities in the computation of the exponential shape functions of the *IIFE*;
- In the case of distributed or concentrated loads, the convergence rate relevant to warping intensities of the steel components is much lower than that relevant to the other response parameters; differences in the convergence rate attenuate in the cases of prestressing or concrete shrinkage.

Provided that a proper discretization of the beam axis is used, depending on the adopted finite element, the beam model is able to capture very well the structural response of composite beams subjected to different loads and restraint conditions obtained from a refined 3D model. In particular, both displacements, stresses, and stress resultants of the 3D model are reproduced by the proposed beam model, which foresees a number of dofs about thirty times lower.

Author Contributions: Conceptualization, G.L. and F.G.; methodology, G.L., F.G., and S.C.; software, F.G. and S.C.; validation, G.L. and F.G.; formal analysis, G.L., F.G., and S.C.; data curation, S.C.; writing—original draft preparation, F.G. and S.C.; writing—review and editing, G.L. and F.G.; visualization, F.G. and S.C.; supervision, L.D. All authors have read and agreed to the published version of the manuscript.

Funding: This research received no external funding.

Data Availability Statement: The data presented in this study are available on request from the corresponding author.

Conflicts of Interest: The authors declare no conflict of interest.

Appendix A

Stress Resultants and Inertial Components

The complete (i.e., non-compact) form of balance conditions (17), which includes stress resultants of the beam components as well as external stresses and forces, assumes the form

$$\begin{array}{c}\int_0^L \left[(\boldsymbol{F}_c+\boldsymbol{F}_r)\cdot\hat{\boldsymbol{w}}_c' + \boldsymbol{S}_{cx}\cdot\hat{\boldsymbol{w}}_c + \boldsymbol{S}_{cy}\cdot\hat{\boldsymbol{w}}_c + \boldsymbol{F}_s\cdot\hat{\boldsymbol{w}}_s' + \boldsymbol{S}_{s\xi}\cdot\hat{\boldsymbol{w}}_s + V\ \hat{v}_0'\right]\, dz \ +\ \int_0^L q\ (\hat{\boldsymbol{w}}_s\cdot\bar{\boldsymbol{a}}_s - \hat{\boldsymbol{w}}_c\cdot\bar{\boldsymbol{a}}_c) dz \\ =\ \int_0^L (\boldsymbol{p}_{cz}\cdot\hat{\boldsymbol{w}}_c\ +\ \boldsymbol{p}_{sz}\cdot\hat{\boldsymbol{w}}_s\ +\ p_y\cdot\hat{v}_0) dz\ +\ (\boldsymbol{P}_{czff}\cdot\hat{\boldsymbol{w}}_c\ +\ \boldsymbol{P}_{szff}\cdot\hat{\boldsymbol{w}}_s\ +\ P_{ya}\cdot\hat{v}_0)|_{\alpha=0,L}\end{array} \tag{A1}$$

where

$$\boldsymbol{F}_c = \int_{A_c} \sigma_{cz}\ \boldsymbol{a}_c\ dA = \begin{bmatrix} N_c \\ M_c \\ W_c \end{bmatrix} \tag{A2}$$

$$\boldsymbol{S}_{cx} = \int_{A_c} \tau_{cxz}\ \boldsymbol{a}_{c,x}\ dA = \begin{bmatrix} 0 \\ 0 \\ Q_{cx} \end{bmatrix} \tag{A3}$$

$$\boldsymbol{S}_{cy} = \int_{A_c} \tau_{cyz}\ \boldsymbol{a}_{c,y}\ dA = \begin{bmatrix} 0 \\ V_c \\ 0 \end{bmatrix} \tag{A4}$$

$$\boldsymbol{F}_r = \int_{A_r} \sigma_{rz}\ \boldsymbol{a}_c\ dA = \begin{bmatrix} N_r \\ M_r \\ W_r \end{bmatrix} \tag{A5}$$

$$\boldsymbol{F}_s = \sum_{i=1}^{n} t_i \int_0^{l_i} \sigma_{sz}\, \boldsymbol{a}_s\, d\xi_i = \begin{bmatrix} N_s \\ M_s \\ W_{sy} \\ W_{sx} \end{bmatrix} \tag{A6}$$

$$\boldsymbol{S}_{s\xi} = \sum_{i=1}^{n} t_i \int_0^{l_i} \tau_{s\xi z}\, \boldsymbol{a}_{s,\xi}\, d\xi_i = \begin{bmatrix} 0 \\ V_s \\ Q_{sy} \\ Q_{sx} \end{bmatrix} \tag{A7}$$

$$\boldsymbol{S}_{s\xi} = \sum_{i=1}^{n} t_i \int_0^{l_i} \tau_{s\xi z}\, \boldsymbol{a}_{s,\xi}\, d\xi_i = \begin{bmatrix} 0 \\ V_s \\ Q_{sy} \\ Q_{sx} \end{bmatrix} \tag{A8}$$

are the generalized stress resultants,

$$\boldsymbol{p}_{cz} = \int_{A_c \cup A_r} b_z\, \boldsymbol{a}_c\, dA + \int_{\partial A_c \cup \partial A_r} s_z\, \boldsymbol{a}_c\, dl = \begin{bmatrix} q_{cz} \\ m_{cx} \\ \omega_{cy} \end{bmatrix} \tag{A9}$$

$$\boldsymbol{p}_{cz} = \int_{A_c \cup A_r} b_z\, \boldsymbol{a}_c\, dA + \int_{\partial A_c \cup \partial A_r} s_z\, \boldsymbol{a}_c\, dl = \begin{bmatrix} q_{cz} \\ m_{cx} \\ \omega_{cy} \end{bmatrix} \tag{A10}$$

$$q_y = \int_{A_c \cup A_r} b_y\, dA + \int_{\partial A_c \cup \partial A_r} s_y\, dl + \sum_{i=1}^{n} t_i \int_0^{l_i} \mathrm{b_y}\, d\xi_i + \sum_{i=1}^{n} \int_0^{l_i} \mathrm{s_y}\, d\mathrm{l} \tag{A11}$$

are the resultants of forces applied along the beam, and

$$\boldsymbol{P}_{cz\alpha} = \int_{(A_c \cup A_r)_\alpha} s_z\, \boldsymbol{a}_c\, dA = \begin{bmatrix} F_{cz\alpha} \\ M_{cx\alpha} \\ W_{cy\alpha} \end{bmatrix} \qquad con\ \alpha = 0, L \tag{A12}$$

$$\boldsymbol{P}_{sz\alpha} = \int_{(A_s)_\alpha} s_z\, \boldsymbol{a}_s\, dA = \begin{bmatrix} F_{sz\alpha} \\ M_{sx\alpha} \\ W_{sx\alpha} \\ W_{sy\alpha} \end{bmatrix} \qquad con\ \alpha = 0, L \tag{A13}$$

$$Q_{y\alpha} = \int_{(A_c \cup A_r)_\alpha} s_y\, dA + \int_{(A_s)_\alpha} s_y\, dA \qquad con\ \alpha = 0, L \tag{A14}$$

are the resultants of the forces applied at the beam end cross sections. Inertia of the beam cross section, constituting the global stiffness matrix $\boldsymbol{K}$, is

$$\boldsymbol{I}_c = \int_{A_c} \boldsymbol{a}_c \otimes \boldsymbol{a}_c\, dA \tag{A15}$$

$$\boldsymbol{J}_c = \int_{A_c} \boldsymbol{a}_{c,x} \otimes \boldsymbol{a}_{c,x} + \boldsymbol{a}_{c,y} \otimes \boldsymbol{a}_{c,y}\, dA \tag{A16}$$

$$\boldsymbol{L}_c = \int_{A_c} \boldsymbol{a}_{c,y}\, dA \tag{A17}$$

$$\boldsymbol{I}_r = \int_{A_r} \boldsymbol{a}_c \otimes \boldsymbol{a}_c\, dA \tag{A18}$$

$$\boldsymbol{I}_s = \sum_{i=1}^{n} t_i \int_0^{l_i} \boldsymbol{a}_s \otimes \boldsymbol{a}_s\, d\xi_i \tag{A19}$$

$$\boldsymbol{J}_s = \sum_{i=1}^{n} t_i \int_0^{l_i} \boldsymbol{a}_{s,\xi} \otimes \boldsymbol{a}_{s,\xi}\, d\xi_i \tag{A20}$$

$$\boldsymbol{L}_s = \sum_{i=1}^{n} t_i \int_0^{l_i} \boldsymbol{a}_{s,\xi}\, y_{,\xi}\, d\xi_i \tag{A21}$$

$$m_s = \sum_{i=1}^{n} t_i \int_0^{l_i} y_{,\xi}^2\, d\xi_i \tag{A22}$$

$$\boldsymbol{A}_{\alpha\beta} = \overline{\boldsymbol{a}}_\alpha \otimes \overline{\boldsymbol{a}}_\beta \qquad \alpha, \beta = c,\ s \tag{A23}$$

Appendix B

Stress State

Stresses of Equations (9)–(11), relevant to strains descending from the admissible displacement field according to constitutive relationships, are usually referred to as active stresses and can be used to compute normal longitudinal stresses σ_{cz}, σ_{sz}, and σ_{rz} with negligible errors (Equations (9)–(11)). However, active stresses do not satisfy the local equilibrium, which also requires additional non-vanishing stress components, called reactive stresses. The latter do not appear in the virtual work theorem expression and can be estimated by means of the local equilibrium conditions. These components are significant in the case of shear stresses. By assuming concrete and steel members as thin-walled elements, the total shear stresses τ_{cxz} and $\tau_{s\xi z}$ may be calculated separately for the concrete slab and the steel girder, starting from the local equilibrium. For the steel girder, by considering the constitutive law in Equation (10), the local equilibrium condition with null body forces provides

$$\sigma'_{sz} + \tau_{s\xi z,\ \xi} = 0 \tag{A24}$$

which, integrated along the local curvilinear abscissa ξ, yields

$$\tau_{s\xi z}(\xi, z) = \widetilde{\tau}_{s\xi z} - \mathrm{E_s}\, \boldsymbol{w}''_s \int_0^{\xi} \boldsymbol{a}_s d\xi + \mathrm{E_s} \int_0^{\xi} \overline{\varepsilon}'_{sz}\, d\xi \tag{A25}$$

Equation (A25) is valid for each wall of the steel girder; $\widetilde{\tau}_{s\xi z}$ is an integration constant that has to be evaluated by imposing equilibrium conditions at the wall edges. As for the concrete slab, reinforcements are assumed to be smeared within the slab so that shear stress discontinuities only occur at the slab–girder connection. Thus, the slab is divided into different panels, each one characterised by a curvilinear abscissa ξ and by the relevant shear stresses $\tau_{c\xi z}$. The local equilibrium condition is provided by the following relationship:

$$\int_{h_c} \sigma'_{cz} dy + \int_{h_r} \sigma'_{rz}\, dy + \tau_{c\xi z,\ \xi}\, h_c = 0 \tag{A26}$$

where h_c is the thickness of the slab and h_r is the notional thickness of the smeared reinforcements. By considering constitutive laws in Equation (9) and Equation (11), integration along the local abscissa ξ yields

$$\begin{aligned} \tau_{c\xi z}(\xi, z) = \widetilde{\tau}_{c\xi z} \quad & -\tfrac{1}{h_c}\mathrm{E}_c\, \boldsymbol{w}''_c \int_0^{\xi} \int_{h_c} \boldsymbol{a}_c d\xi dy + \tfrac{1}{h_c}\mathrm{E_c} \int_0^{\xi} \int_{h_c} \overline{\varepsilon}'_{cz}\, d\xi dy \\ & -\tfrac{1}{h_c}\mathrm{E}_r\, \boldsymbol{w}''_c \int_0^{\xi} \int_{h_r} \boldsymbol{a}_c d\xi dy + \tfrac{1}{h_c}\mathrm{E_r} \int_0^{\xi} \int_{h_r} \overline{\varepsilon}'_{rz} d\xi dy \end{aligned} \tag{A27}$$

where, analogously to the steel girder, $\widetilde{\tau}_{s\xi z}$ is an integration constant that has to be evaluated by imposing equilibrium conditions at the wall edges.

Appendix C

Notations

The following symbols are used in this paper:

0	origin of Cartesian coordinate system;
$\boldsymbol{A}$	matrix containing stiffnesses of the beam cross section;
A	area;
$\boldsymbol{a}$	geometric vector;
$\boldsymbol{B}$	matrix containing stiffnesses of the beam cross section;
$\boldsymbol{b}$	vector of the integration constants;
B	concrete slab width;
$\boldsymbol{C}$	matrix containing stiffnesses of the beam cross section;
$\boldsymbol{c}$	vector of loads and stress-independent strain along the beam;
$\boldsymbol{d}$	vector of all unknown displacements;
d	differential operator;
$\boldsymbol{E}$	exponential matrix;
E	Young's modulus;
$\boldsymbol{f}$	vector of nodal forces;
f_c, f_{sh}, f_{sv}	warping intensity functions;
G	shear modulus;
h_c	slab thickness;
$\boldsymbol{I}$	inertia matrix or identity matrix;
$\boldsymbol{J}$	inertia matrix;
$\boldsymbol{K}$	stiffness matrix of the beam element;
k, i	indexes;
L	length of the beam;
l	length of the beam plane walls;
l_e	length of the finite element;
$\boldsymbol{L}$	inertia matrix;
M	bending moment at the beam end cross section;
m	bending moment along the beam axis;
N	longitudinal force at the beam end cross section;
$\boldsymbol{N}_e$	matrix of interpolating functions;
$\overline{\boldsymbol{n}}$	vector of resultants of forces due to restrained stress-independent strain;
n	number of the plane steel walls;
n_e	number of finite elements
$\boldsymbol{p}$	resultants of external forces along the beam axis;
$\boldsymbol{P}$	resultants of external forces at the beam end cross section;
Q_v	resultant of vertical loads at the beam end cross section;
q_c, q_s	longitudinal forces along the beam axis;
q_v	resultant of vertical loads along the beam axis;
$\boldsymbol{R}$	inverse of matrix of exponential matrices evaluated at beam ends;
$\boldsymbol{s}$	vector grouping unknown displacements and their first derivative;
t_i	thickness of the i-th plane steel wall;
$\cup$	linear matrix operator;
$\boldsymbol{U}$	displacement of the two end cross sections of the beam;
$\boldsymbol{u}$	displacement of the end cross section of the beam;
u	transverse displacement, along coordinate direction X;
$\boldsymbol{v}_e$	vector of the unknown nodal displacements;
$\boldsymbol{v}$	assembled vector of the nodal displacements of all the elements;
v	vertical displacement of the cross section, along coordinate direction Y;
W	bi-moment at the beam end cross section;
w	longitudinal displacement, along coordinate direction Z;
$\boldsymbol{w}$	vector grouping the generalised displacements;
X, Y, Z	coordinate axes;
x, y, z	coordinates;
$\overline{x}$, $\overline{y}$	coordinates of the slab–girder interface connection;
α	direction cosine of the local abscissa;

ϵ, k, μ	overall stress-independent strain;
$\bar{\boldsymbol{\varepsilon}}$	vector of stress-independent strains;
$\bar{\varepsilon}$	stress-independent strain;
$\widetilde{\varepsilon}$	generic nonlinear stress-independent longitudinal strain field;
Φ	rotation;
Γ	beam–slab interface slip;
η	local abscissa of the finite element;
λ	normalised abscissa of the finite element
μ	interpolating function;
ν	Poisson's ratio; interpolating function
ρ	stiffness per-unit-length of the shear connection;
σ_z	normal stress;
τ	shear stress;
v	interpolating function;
ω	bi-moment along the beam axis;
ξ	local abscissa of the beam plane walls;
ψ_c	slab warping function;
ψ_{sh}	steel warping function due to longitudinal shear flow;
ψ_{sv}	steel warping function due to shear force.
Subscripts	
c	concrete part of the composite beam;
e	finite element;
r	steel reinforcement part of the composite beam;
s	steel part of the composite beam;
0	referred to the origin of coordinate system;
,	partial derivatives.
Symbols and Superscripts	
T	concrete part of the composite beam;
$'$	derivative with respect to z variable;
$\mathcal{D}$	formal linear differential operator;
$\hat{}$	variation;
$\cdot$	scalar product.

References

1. European Committee for Standardization (CEN). *Eurocode 4: Design of Composite Steel and Concrete Structures–Part 2: Rules for Bridges*; EN1994-2; CEN: Brussels, Belgium, 2005.
2. Newmark, N.M.; Siess, C.P.; Viest, I.M. Test and analysis of composite beams with incomplete interaction. *Proc. Soc. Exp. Stress Anal.* **1951**, *9*, 75–92.
3. Nguyen, Q.H.; Hjiaj, M.; Uy, B. Time-dependent analysis of composite beams with partial interaction based on time-discrete exact stiffness matrix. *Eng. Struct.* **2010**, *32*, 2902–2911. [CrossRef]
4. Ranzi, G.; Bradford, M.A. Analysis of composite beams with partial interaction using the direct stiffness approach accounting for time effects. *Int. J. Numer. Methods Eng.* **2009**, *78*, 564–586. [CrossRef]
5. Gara, F.; Ranzi, G.; Leoni, G. Time analysis of composite beams with partial interaction using available modelling techniques: A comparative study. *J. Constr. Steel Res.* **2006**, *62*, 917–930. [CrossRef]
6. Dezi, L.; Gara, F.; Leoni, G. Construction sequence modelling for continuous steel-concrete composite decks. *Steel Compos. Struct.* **2006**, *6*, 123–138. [CrossRef]
7. Gara, F.; Leoni, G.; Dezi, L. Slab cracking control in continuous steel-concrete bridge decks. *J. Bridge Engrg. ASCE* **2013**, *18*, 1319–1327. [CrossRef]
8. Ranzi, G.; Bradford, M.A. Nonlinear analysis of composite beams with partial shear interaction by means of the direct stiffness method. *Steel Compos. Struct.* **2009**, *9*, 131–158. [CrossRef]
9. Virtuoso, F.; Vieira, R. Time dependent behaviour of continuous composite beams with flexible connection. *J. Constr. Steel Res.* **2004**, *60*, 451–463. [CrossRef]
10. Dall'Asta, A.; Zona, A. Three-field mixed formulation for the non-linear analysis of composite beams with deformable shear connection. *Finite Elem. Anal. Des.* **2004**, *40*, 425–448. [CrossRef]
11. Gara, F.; Ranzi, G.; Leoni, G. Displacement-based formulations for composite beams with longitudinal slip and vertical uplift. *Int. J. Numer. Methods Eng.* **2006**, *65*, 1197–1220. [CrossRef]
12. Ranzi, G.; Gara, F.; Ansourian, P. General method of analysis for composite beams with longitudinal and transverse partial interaction. *Comput. Struct.* **2006**, *84*, 2373–2384. [CrossRef]

13. Taig, G.; Ranzi, G. Generalised beam theory for composite beams with longitudinal and transverse partial interaction. *Math. Mech. Solids* **2017**, *22*, 2011–2039. [CrossRef]
14. Nguyen, Q.H.; Hjiaj, M.; Guezouli, S. Exact finite element model for shear-deformable two layer beams with discrete shear connection. *Finite Elem. Anal. Des.* **2011**, *47*, 718–727. [CrossRef]
15. da Silva, A.R.; Sousa, J.B.M. A family of interface elements for the analysis of composite beams with interlayer slip. *Finite Elem. Anal. Des.* **2009**, *45*, 305–314. [CrossRef]
16. Gara, F.; Leoni, G.; Dezi, L. A beam finite element including shear lag effect for the time dependent analysis of steel–concrete composite decks. *Eng. Struct.* **2009**, *31*, 1888–1902. [CrossRef]
17. Timoshenko, S. Theory of bending, torsion and buckling of thin walled members of open section. *J. Frankl. Inst.* **1945**, *239*, 249–268. [CrossRef]
18. Xu, R.; Wang, G. Bending solutions of the Timoshenko partial-interaction composite beams using Euler-Bernoulli solutions. *J. Eng. Mech. ASCE* **2013**, *139*, 1881–1885. [CrossRef]
19. Vo, T.P.; Thai, H.T. Static behaviour of composite beams using various refined shear deformation theories. *Comp. Struct.* **2012**, *94*, 2513–2522. [CrossRef]
20. Zona, A.; Ranzi, G. Finite element models for nonlinear analysis of steel–concrete composite beams with partial interaction in combined bending and shear. *Finite Elem. Anal. Des.* **2011**, *47*, 98–118. [CrossRef]
21. Ranzi, G.; Zona, A. A steel–concrete composite beam model with partial interaction including the shear deformability of the steel component. *Eng. Struct.* **2007**, *29*, 3026–3041. [CrossRef]
22. Schnabl, S.; Saje, M.; Turk, G.; Planinc, I. Analytical solution of two-layer beam taking into account interlayer slip and shear deformation. *J. Struct. Eng.* **2007**, *133*, 886–894. [CrossRef]
23. Dezi, L.; Gara, F.; Leoni, G.; Tarantino, M.A. Time dependent analysis of shear-lag effect in composite beams. *J. Engrg. Mech. ASCE* **2001**, *127*, 71–79. [CrossRef]
24. Dezi, L.; Gara, F.; Leoni, G. Shear-Lag effect in twin-girder composite decks. *Steel Compos. Struct.* **2003**, *3*, 111–122. [CrossRef]
25. Dezi, L.; Gara, F.; Leoni, G. Effective slab width in prestressed twin-girder composite decks. *J. Struct. Engrg. ASCE* **2006**, *132*, 1358–1370. [CrossRef]
26. Macorini, L.; Fragiacomo, M.; Amadio, C.; Izzuddin, B.A. Long-term analysis of steel–concrete composite beams: FE modelling for effective width evaluation. *Eng. Struct.* **2006**, *28*, 1110–1121. [CrossRef]
27. Gara, F.; Ranzi, G.; Leoni, G. Partial interaction analysis with shear-lag effects of composite bridges: A finite element implementation for design applications. *Adv. Steel Constr.* **2011**, *7*, 1–16.
28. Gara, F.; Ranzi, G.; Leoni, G. Analysis of the shear lag effect in composite bridges with complex static schemes by means of a deck finite element. *Int. J. Steel Struct.* **2008**, *8*, 249–260.
29. Gonçalves, R.; Camotim, D. Steel-concrete composite bridge analysis using Generalised Beam Theory. *Steel Compos. Struct.* **2010**, *10*, 223–243. [CrossRef]
30. Gara, F.; Leoni, G.; Carbonari, S.; Dezi, L. A higher order steel-concrete composite beam model. *Eng. Struct.* **2014**, *80*, 260–273. [CrossRef]
31. Chakrabarti, A.; Sheikh, A.H.; Grifith, M.; Oehlers, D.J. Analysis of composite beams with longitudinal and transverse partial interactions using higher order beam theory. *Int. J. Mech. Sci.* **2012**, *59*, 115–125. [CrossRef]
32. Computer and Structures, Inc. *CSI Analysis Reference Manual*; SAP 2000; Computer and Structures, Inc.: Berkeley, CA, USA, 2011.
33. Reddy, J.N. On locking-free shear deformable beam finite elements. *Comput. Methods Appl. Mech. Engrg.* **1997**, *149*, 113–132. [CrossRef]
34. Moler, C.; Van Loan, C. Nineteen Dubious Ways to Compute the Exponential of a Matrix, Twenty-Five Years Later. *SIAM Rev.* **2003**, *45*, 3–49. [CrossRef]